NASA Contractor Report 187049

Theory of Finite Disturbances in a Centrifugal Compression System with a Vaneless Radial Diffuser

F.K. Moore
Cornell University
Ithaca, New York

December 1990

Prepared for
Lewis Research Center
Under Grant NAG3-349

National Aeronautics and
Space Administration

TABLE OF CONTENTS

1. INTRODUCTION

The present paper extends a previous analysis [1] of weak rotating waves in a centrifugal compression system with a vaneless diffuser, shown in Fig. 1.1 adapted from that paper. Conditions were found for the existence of permanent rotating waves of small amplitude. The theory assumed an inviscid flow process in the vaneless diffuser. Waves of "fast" and "slow" types were found, consistent with experimental experience.

The slow waves (usually called "diffuser stall" in the literature) are especially interesting in that resonance was found. That is, when flow coefficient Φ is reduced, a value is suddenly reached for which pressure amplitude may be arbitrarily large, for a given radial-flow disturbance of a given mode. Fig. 1.2 from [1] shows the real part of a presumed pressure disturbance, and the corresponding slow-wave speed coefficient. Negative values of the indicated function presumably represent amplification, but that could not be proved in the linearized analysis. This predicted resonant behavior is consistent with experiments, and is quite unlike anything found in the corresponding problem of axial system stall [2]. The present paper begins with remarks showing how the results of [1] can be reconciled with experimental evidence [3] of an effect of diffuser width on the occurrence of rotating stall.

The weak-wave analysis cannot, of course, predict limit cycles, nor can it predict what will actually happen when flow coefficient is reduced through the resonant condition. The wave cannot remain weak and permanent (the only permitted linear solution); neither can its amplitude be infinite. It must grow, and yet disturbances must physically remain finite. Clearly, the next step should be a nonlinear analysis, and the appropriate approach would seem to be that of [4].

Therefore, the pressure and mass balance equations for the centrifugal system are first developed, as in [4]. A Galerkin procedure is applied, also as in [4], for an assumed single rotating mode, and the corresponding dynamic pressure rise in the diffuser is found to second order in disturbance amplitude. Subject to certain assumptions to be described, a final set of equations is derived, which govern a rather general transient comprised of surge-like and rotating-wave disturbances in combination. In the solution of these equations, use may be made of the linear solutions for velocity and pressure disturbance already found in [1].

Then, an ideal example problem is solved with these equations, and it is shown how resonance is traversed when flow coefficient is decreased

(throttled). In effect, a surge transient must generally occur near resonance, so that the wave amplitudes, though singular, remain finite.

Away from resonant conditions, the possibility of more than one wave type should be considered, because two families of rotating waves (fast and slow) are in principle allowed. This problem is discussed.

2. EFFECT OF DIFFUSER WIDTH

The assumption of inviscid flow in [1] and this Report may be questioned in view of the known effects of Reynolds number on performance and stability of the machines under discussion [3,4]. In most flow problems, however, it is important to know what inviscid analysis has to tell; that knowledge avoids the pitfall of ascribing puzzling flow observations, especially instabilities, to viscous phenomena such as separation, when the real cause may lie elsewhere. It is believed that the present study shows an inviscid basis for rotating instabilities found with vaneless diffusers.

Diffuser width has no effect in the present theory, yet experiments, reviewed and analyzed in [3], show a clear tendency for increased diffuser width to increase the critical flow coefficient for instability. Fig. 35 of [3] indicates that when width l increases from 2 percent to 15 percent of exit radius r_F, the critical flow coefficient increases from about 0.10 to about 0.25. An asymptote of perhaps 0.28 is apparently approached as l is increased further. Fig. 1.2 (Fig. 10 of [1]), on the other hand, gives a critical flow coefficient of about 0.3; thus the inviscid analysis agrees with the asymptotic value for large l suggested by [3]. The influence of radius ratio will be different in [1] and [3], because the discharge is different. In any case, a larger radius ratio leads to a higher critical flow coefficient in both theory and experiment. The variation with width must obviously be an effect of viscosity, which was not considered in [1].

Fig. 36 of [3] also suggests that the foregoing critical flow coefficients are valid for Reynolds number (based on l and on impeller exit velocity) of 10^5, but should be increased by about 0.07 for 10^4 and decreased a like amount for 10^6.

Boundary-Layer Displacement and Diffuser Convergence

To explain these results in terms of the present theory, one should first consider the displacement effect of the wall boundary layers in the diffuser. The sketch (Fig. 2.1) shows a narrow and a wide diffuser, each with the same growing boundary layers and hence the same displacement effects. Clearly, the narrow diffuser will effectively be more convergent because of the boundary-layer displacement effect.

Convergence effect was discussed in [1], and was expressed as a power law (See Fig. 9 of [1])

$$l = l_1 \, r^{-n} \qquad (2.1)$$

Results shown in Fig. 10 of [1] showed that the critical flow coefficient (in the first circumferential mode) was lower for a convergent case (n= 1) than for the parallel-wall case (n = 0). Subsequent calculations give the same result for the higher modes (3rd and 4th) which are the most unstable. Figs. 2.2 and 2.3 show the pertinent results. Thus, convergence due to boundary-layer displacement would be predicted to cause a lowered critical flow coefficient for a narrow diffuser compared with a wide one. Of course, when the width is much greater than the boundary-layer thickness, further increasing the width will have no effect. One may consider that the present inviscid theory assumes infinite diffuser width, in effect.

The foregoing discussion is qualitative; to make numerical predictions, or to explain the Reynolds number correction also suggested in [3], would require quantitative knowledge of the displacement thickness and how it varies with Reynolds number. That information cannot readily be inferred from the literature.

The theory predicts that a more convergent diffuser will be more stable, whether the convergence is due to displacement effect or is simply a geometrical feature of the diffuser. It would therefore appear advantageous to build the diffuser with a convergent shape. However, pressure rise in such a diffuser would be more gradual, and to achieve the same final pressure ratio, its exit radius would have to be larger. A larger exit radius, in itself, is destabilizing. For the third circumferential mode and parallel diffuser walls (n = 0), the critical flow coefficient is 0.180, if r_F is 1.6. If the walls are to be convergent to the degree that n = 1, but the pressure-rise coefficient is kept the same, then one finds that r_F must be 1.89 instead of 1.6. For r_F = 1.89 and n= 1, the critical flow coefficient turns out to be 0.175, which is virtually the same as that for the shorter, parallel-wall diffuser. Therefore, it would seem that if pressure coefficient is held constant by changing exit radius, convergence of the diffuser has negligible effect on stability.

Details of Linearized Analysis

Owing to length restrictions, equations and formulas which included the effects of convergence and mode number were not presented in [1]. For the record, Appendix A of this Report collects those details, thereby generalizing the Eqs. (9 through 20) which appear in [1]. The relevant discussions and arguments appear in [1] and need not be repeated in the Appendix.

3. TRANSIENT EQUATIONS

Pressure and Mass Balances of System

The overall pressure balance of an axial compression system appears in Eq. (42) of [4], and is repeated here for reference:

$$\Psi(\xi) + l_c\,\Phi_\xi = \Psi_c\,(\Phi + g) - mY_\xi + \frac{1}{2a}\,(2Y_{\xi\theta\theta} + Y_{\theta\theta}) \tag{3.1}$$

For the centrifugal system of present interest, shown in Fig. 1.1, the corresponding equation may easily be derived:

$$\Psi + l_c\,\Phi_\xi = \Psi_c(\Phi+g) - mY_\xi + \frac{1}{2a}\,(Y_{\xi\theta\theta} + Y_{\theta\theta\theta}) - [dP_1 + (\bar{P}_1 - \bar{P}_{gs1})] \tag{3.2}$$

(a) (b) (c) (d) (e) (f)

The terms of this equation are lettered, and will be discussed in turn, making reference to the corresponding terms of Eq. (3.1).

(a) The total-to-static pressure-rise coefficient of the entire system is

$$\Psi = (p_F - p_T)/\rho U^2 \tag{3.3}$$

where p_T is considered constant, while the plenum pressure p_F to which the diffuser discharges may be a function of time. The rotor tip velocity is denoted by U.

(b) As in Eq. (3.1), the second term describes flow inertia up to the rotor exit, based on the coefficient Φ of circumferentially-averaged radial velocity there. The dimensionless length l_c is now

$$l_c = l_I\,\frac{A_{f1}}{A_{f0}} + \frac{1}{2a}\,; \quad a = r_1/\tau U \tag{3.4}$$

Unlike the axial case, the inlet velocity differs from the rotor exit velocity used as reference, and, by continuity, goes inversely with flow area A_F. Therefore, the area ratio A_{f1}/A_{f0} now appears. If τ is defined as in Eq. (2) of [4], then a new factor of 1/2 appears in Eq. (3.4) because there is no stator in the present case, whereas [4] assumed a two-row (rotor-stator) stage. The time coordinate is ξ, relative to time for the rotor to travel one radian.

(c) As usual [4], the axisymmetric, quasi-steady pressure-rise coefficient is denoted by Ψ_c, stipulated to include the pressure rise in the diffuser, which is written as $-\bar{P}_{qs1}$)

(d) As discussed in [4], the function $Y(\xi,\theta)$ is the potential for any wave-like velocity disturbance, depending only on ξ and θ; such a disturbance is assumed "straight through", not a function of position along the flow path from entrance to exit. Corresponding to [4], the disturbance of radial flow coefficient at exit is denoted by g, and

$$\phi = \Phi + g \; ; \quad g = - Y_{\theta\theta} \tag{3.5}$$

The term (d) specifically refers to the pressure change caused at the entrance by the appearance of a transverse (that is, circumferential) velocity disturbance (w) there, which is in turn induced by the axial disturbance described by g. The assumption of [4] is carried over, that w and g are related as if the flow were potential and harmonic at the entrance. The applicable relations are

$$w_1 = U \frac{A_{f1}}{A_{f0}} Y_\theta \; ; \quad m = \frac{1}{r_F} \frac{A_{f1}}{A_{f0}} \tag{3.6}$$

Again, the area ratio A_{f1}/A_{f0} appears, because the disturbance function g is defined at the rotor exit, while Eq. (3.6) refers to events at the entrance. The radius ratio r_F also appears as a scaling for the potential function at the entrance, because all distances have been referred to the exit radius.

(e) This term is the same as the corresponding term of Eq. (3.1) with a factor of 2 omitted. That difference reflects the presence of only one blade row, while the axial case [4] has two.

(f) The last group of terms is new to the centrifugal case, and refers to the pressure in the vaneless diffuser. A pressure coefficient in the diffuser is defined below, and may be assumed to consist of an angle-averaged part (perhaps unsteady) $\bar{P}$ and a wave-like part $_dP$ (whose angle average is zero).

$$\frac{p-p_F}{\rho U^2} = P = \bar{P}(r,\xi) + {}_dP(r,\xi,\theta) \tag{3.7}$$

Now, the axisymmetric overall pressure rise function ψ_c , presumed known, includes quasi-steady pressure rise - $\bar{P}_{qs1}(\Phi)$ from diffuser entrance to exit. Therefore that quantity must appear in the group (f), so that Eq. (3.2) is satisfied in the axisymmetric quasi-steady case, when $\Psi = \psi_c$ and all its other terms must vanish by definition.

In the postulated system (Fig. 1.1), pressure falls from plenum to exhaust through a throttle. The throttle has a characteristic performance function F_T, presumed known, just as does the compressor:

$$\Psi = F_T(\Phi_T) \tag{3.8}$$

The flow coefficient Φ_T may differ from Φ because mass may accumulate in the plenum. In fact, with the plenum regarded as an isentropic air spring, Eq. (36) of [24] applies:

$$l_c \Psi_\xi = \frac{1}{4B_g^2}(\Phi - \Phi_r) \tag{3.9}$$

Eqs. (3.2), (3.8), and (3.9) constitute the governing equations for disturbances to be considered. The problem is to find permitted solutions for $\Psi(\xi)$, $\Phi(\xi)$, $Y(\xi,\theta)$, and corresponding pressure distributions in the diffuser. First, of course, the throttle and compressor characteristics must be specified.

Galerkin Version with Cubic Characteristic

As in [4], the system is greatly simplified by use of the Galerkin procedure, which represents the periodic functions $Y(\xi,\theta)$, and for the present problem, also ${}_dP(r,\xi,\theta)$, as harmonic functions with only their time-dependent amplitudes remaining unknown. It is assumed that Y(or the related g) can be well represented by waves traveling at dimensionless speed f in the positive θ-direction; thus, as in Eq. (58) of [4],

$$g = W A_1 \cos \tilde{\theta} \tag{3.10}$$

and

$$P = \bar{P}(r,\xi) + {}_1P(r,\xi)\cos\tilde{\theta} + {}_2P(r,\xi)\sin\tilde{\theta} \qquad (3.11)$$

where two new functions of radius and time, ${}_1P$ and ${}_2P$ have been used to construct ${}_dP$, and where

$$\tilde{\theta} = \theta - f\xi \qquad (3.12)$$

Two major questions may be raised about this use of the Galerkin method. First, there may be more than one type of wave represented at a given time; Ref. [1] shows that there are "fast" and "slow" wave types and also higher harmonics in the centrifugal, but not the axial, case. These complications can easily be dealt with in the present analysis, as will be shown later. The second question is more fundamental; waves in this nonlinear problem may differ substantially in shape from the simple harmonic form. Fig. 5 of [4] shows this difference for the axial problem. No such comparison can be made for the centrifugal case; the necessary exact nonlinear solution of the diffuser flow is not available. However, wave traces measured in centrifugal machines [3] seem to look rather more harmonic than is usual in axial machines, perhaps because of a smoothing effect of the diffuser. Therefore, one may be optimistic about the accuracy of the Galerkin method for the centrifugal problem.

The Galerkin method is especially needed in the present problem because of the need to provide a nonlinear solution for flow in the diffuser, whereas in the corresponding axial problem, the only nonlinearities arise in the compressor and throttle characteristic functions.

It is further assumed that the compressor characteristic is well represented by a cubic function, namely

$$\psi_c = \psi_o + H\left[\frac{3}{2}\,\frac{\Phi - S + g}{W} - \frac{1}{2}\left(\frac{\Phi - S + g}{W}\right)^3\right] \qquad (3.13)$$

This function, shown in Fig. 3.1, has one more parameter (S) than the corresponding cubic for axial systems (Fig. 3 of [4]). Because measured characteristics for centrifugal machines tend to be very smooth functions, the assumed cubic representation should be very satisfactory. The throttle characteristic might be a simple quadratic, also illustrated in Fig. 3.1.

To carry out the Galerkin procedure, one first substitutes Eqs. (3.5), (3.10), (3.11), and (3.15) into Eq. (3.2), and then performs three

integrations over a cycle of $\tilde{\theta}$, namely of Eq. (3.2) itself, of Eq. (3.2) multiplied through by $\cos\tilde{\theta}$, and then of Eq. (3.2) multiplied through by $\sin\tilde{\theta}$. The results of these operations are, respectively,

$$\Psi + l_c\Phi_\xi = \psi_c(\Phi) - \frac{3}{4}\frac{H}{W}(\Phi - S)\,A_1^2 - (\bar{P}_1 - \bar{P}_{qs1}) \tag{3.14}$$

$$(m + \frac{1}{2a})\,A_{1\xi} + \frac{H}{W}\left\{\frac{3}{8}A_1^3 - \frac{3}{2}\left[1 - (\frac{\Phi - S}{W})^2\right]A_1\right\} + \frac{1}{W}\,{}_1P_1(\xi) = 0 \tag{3.15}$$

$$\left[(m + \frac{1}{2a})\,f - \frac{1}{2a}\right]A_1 + \frac{1}{W}\,{}_2P_1(\xi) = 0 \tag{3.16}$$

These equations are nearly equivalent to Eqs. (59 through 61) of [4]. The next step must be to analyze the diffuser flow in order to relate the new pressure terms to velocity-disturbance amplitude.

Pressure Disturbance in Diffuser

Flow in the vaneless, parallel-wall diffuser will be considered inviscid, just as it was in [1]. The governing Euler equations, written in original dimensional variables, are

$$v_t + \frac{\partial}{\partial r}\left[\frac{1}{2}(v^2 + w^2) + \frac{p}{\rho}\right] - (\frac{w^2}{r} + ww_r - \frac{wv_\theta}{r}) = 0 \tag{3.17}$$

$$w_t + \frac{1}{r}\frac{\partial}{\partial\theta}\left[\frac{1}{2}(v^2 + w^2) + \frac{p}{\rho}\right] + (\frac{vw}{r} + vw_r - \frac{vv_\theta}{r}) = 0 \tag{3.18}$$

$$v_r + \frac{v}{r} + \frac{1}{r}w_\theta = 0 \tag{3.19}$$

Next, the Galerkin definition of radial velocity disturbance, Eq. (3.10), is generalized to allow for phase change in the diffuser:

$$v = U\left[\frac{\Phi(\xi)}{r} + WA(r, \xi)\cos\tilde{\theta} + WB(r, \xi)\sin\tilde{\theta}\right] \tag{3.20}$$

Using this equation in the continuity equation, Eq. (3.19), one may integrate the latter to find circumferential velocity:

$$w = U\left[\frac{1}{r} - W\,(A + rA_r)\sin\tilde{\theta} + W(B + rB_r)\cos\tilde{\theta} + X(r,\xi)\right. \qquad (3.21)$$

The first term implies rotor blades are radial at rotor exit. The function X represents a swirl of unknown intensity, resulting from integration. The corresponding pressure representation is already in place, as given by Eq. (3.11), with Eq. (3.7) providing the connection with static pressure. The pressure in the diffuser, P_F, may be a function of time, of course, but will disappear when differentiated in Eqs. (3.17) and (3.18).

The applicable boundary conditions in the diffuser are as in [1]. Radial velocity is specified at the diffuser entrance:

$$A(1,\xi) \equiv A_1(\xi)\,; \quad B_1 = 0 \qquad (3.22)$$

Circumferential velocity disturbance vanishes there, and therefore

$$X_1 = 0\,; \quad A_{r_1} = -A_1\,; \quad B_{r_1} = 0 \qquad (3.23)$$

At the diffuser discharge, the pressure disturbance must vanish:

$$\bar{P}_F = {}_1P_F = {}_2P_F = 0 \qquad (3.24)$$

Two further assumptions are now made about the diffuser flow, in order to facilitate solutions; first, that propagation speed f is constant (In problems involving inlet distortion, f is no doubt a function of time), and second, that terms of order the cube of the given disturbance A may be neglected; this means that the square of the unknown swirl X, and products such as AX, may be neglected. The equations resulting from the Galerkin substitutions into Eqs. (3.17) and (3.18) and integration after multiplying by 1, $\cos\tilde{\theta}$, and $\sin\tilde{\theta}$ are six in number:

$$\bar{P}_r = -\frac{1}{r}\Phi_\xi + (1 + \Phi^2)\frac{1}{r^3} + \frac{1}{2}rW^2\,(A_r^2 + B_r^2) + 2W^2\frac{X}{r} \qquad (3.25)$$

$${}_1P_2 = W\left\{-A_\xi - \frac{\Phi}{r}(A_r - \frac{A}{r}) + \frac{1}{r^2}[2rB_r + (1 + fr^2)B]\right\} \qquad (3.26)$$

$$ {}_2P_r = W\{-B_\xi - \frac{\Phi}{r}(B_r - \frac{B}{r}) - \frac{1}{r^2}[2rA_r + (1 + fr^2)A]\} \tag{3.27} $$

$$ 0 = 3(AB_r - BA_r) + r(A B_{rr} - BA_{rr}) + 2[X_\xi + \frac{\Phi}{r^2}(rX)_r] \tag{3.28} $$

$$ {}_1P = W[-r(A + rA_r)_\xi - (1 - fr^2)(B_r + \frac{B}{r}) - \Phi(rA_{rr} + 3A_r + \frac{A}{r})] \tag{3.29} $$

$$ {}_2P = W[-r(B + rB_r)_\xi + (1 - fr^2)(A_r + \frac{A}{r}) - \Phi(rB_{rr} + 3B_r + \frac{B}{r})] \tag{3.30} $$

Even with the Galerkin simplification, the foregoing system involves 6 unknown functions (3 for pressure and 3 for velocity) as well as an eigenvalue (f) to be found.

The desired solution is permitted by a final assumption, namely that the diffuser flow is quasi-steady. That is, one assumes that surge-like changes in the overall system will have a much longer characteristic time than the time required for fluid to traverse the diffuser. For this to be true, l_c must be much greater than 1. There may be cases when this is not true, of course. Under this assumption, all derivatives with respect to ξ may be dropped, and three benefits become apparent:

Linear wave. Eqs. (3.26), (3.27), (3.29), and (3.30) are now identical to those which govern the linear, small-disturbance problem of [1]. Therefore, properly interpreted, the pressure-wave and velocity-wave solutions of [1], including resonant behavior, can be carried over directly to the present nonlinear problem, Eqs. (3.14 through 3.16). Nonlinearity resides only in Eqs. (3.25) and (3.28), which now can be used separately to find $\bar{P}$ and X.

Swirl-function solution. Eq. (3.28) can be integrated to find the swirl function X. The result is

$$ X = \frac{1}{2\Phi} r^2 (BA_r - A B_r) \tag{3.31} $$

A constant of integration vanishes in view of applicable boundary conditions, Eqs. (3.22) and (3.23). This result is consistent with the previous supposition that X is second order in velocity amplitude.

Mean pressure-rise solution. Knowing A, B, and X, Eq. (3.25) can be integrated to find the mean pressure rise function $\bar{P}_1$ needed for Eq. (3.14). One finds

$$\bar{P} = -\frac{1}{2}(1+\Phi^2)\left(\frac{1}{r^2}-\frac{1}{r_F^2}\right)-\frac{1}{2}W^2\int_r^{r_F}\left[r\,(A_r^2+B_r^2)+\frac{2}{\Phi}(BA_r-AB_r)\right]dr \quad (3.32)$$

Integration limits are chosen to make $\bar{P}_F$ vanish, as Eq. (3.24) requires. Obviously, in the quasi-steady, axisymmetric limit Eq. (3.32) reduces to

$$\bar{P}_{qs} = -\frac{1}{2}(1+\Phi^2)\left(\frac{1}{r^2}-\frac{1}{r_F^2}\right) \quad (3.33)$$

For use in the last term of Eq. (3.14), one may write

$$\bar{P}_1 - \bar{P}_{qs1} = -\frac{1}{2}W^2\int_1^{r_F}\left[r\,(A_r^2+B_r^2)+\frac{2}{\Phi}(BA_r-AB_r)\right]dr \quad (3.34)$$

Final Equations for Transient

To write the final transient equations, it is necessary to interpret A , B, $_1P$, and $_2P$, defined in Eqs. (3.11) and (3.20), in terms of quantities found in the small-disturbance analysis of [1]. In that treatment, radial velocity was defined in complex form

$$\frac{v}{U}=\frac{\Phi}{r}+Ae^{i\theta}\,;\qquad A=AR+i\,AM \quad (3.35)$$

and, for convenience,

$$AR_1=1\,;\qquad AM_1=0 \quad (3.36)$$

Therefore, in terms of the known linear solution, Eq. (3.20) should be written

$$\frac{v}{U} = \frac{\Phi}{r} + WA_1 (\hat{A} \cos\tilde{\theta} + \hat{B} \sin\tilde{\theta}) \tag{3.37}$$

with the understanding that

$$\hat{A} = AR \; ; \; \hat{B} = - AM \tag{3.38}$$

In [4], and also in the present analysis, it will prove convenient to express A_1 in terms of its square:

$$J = A_1^2 \tag{3.39}$$

In [1] the complex pressure rise coefficient had the form

$$_dP = (PR + iPM)\, e^{i\tilde{\theta}} \tag{3.40}$$

and therefore, in terms of the previous linear results, Eq. (3.11) should be written

$$_dP = WA_1(\hat{PR} \cos\tilde{\theta} - \hat{PM} \sin\tilde{\theta}) \; ; \quad \hat{PR} = PR \; ; \quad \hat{PM} = PM \tag{3.41}$$

Therefore, where one sees A, B, $_1P$, and $_2P$ in Eqs (3.14 through 3.16), one should write instead $W\sqrt{J}\,\hat{A}$, $W\sqrt{J}\,\hat{B}$, $WJ\;\hat{PR}$, and $-W\sqrt{J}\,\hat{PM}$. This done, one may write the final transient equations as follows:

$$\Psi + l_c \Phi_\xi = \psi_c (\Phi) +$$

$$\frac{1}{2}\left\{W^2 \int_1^{r_F} [r\,(\hat{A}_r^2 + \hat{B}_r^2) + \frac{2}{\Phi}(\hat{B}\hat{A}_r - \hat{A}\hat{B}_r)]dr - \frac{3}{2}\frac{H}{W}(\Phi - S)\right\} J \tag{3.42}$$

$$(m + \frac{1}{2a}))\, J_\xi + \frac{H}{W}\left\{\frac{3}{4} J - 3\left[1 - (\frac{\Phi - S}{W})^2\right] + 2\frac{W}{H}\hat{PR}_1\right\} J = 0 \tag{3.43}$$

$$\Psi_\xi = \frac{W/H}{4B_g^2}\left[\frac{\Phi}{W} - \frac{F_T^{-1}(\Psi)}{W}\right]\frac{H}{l_c} \tag{3.44}$$

$$(m + \frac{1}{2a})\, f - \frac{1}{2a}\, -\hat{P}M_1 = 0 \qquad (3.45)$$

These equations parallel Eqs. (59-61) of [4], but differ in the way wave amplitude appears. For example, pressure amplitude affects rotation speed f in the present case. Most notably, Eq. (3.43) shows that a negative value of the real part of the pressure wave (the part in phase with the radial velocity disturbance), in itself, causes amplitude (J) to grow with time. This confirms expectations of [1]. As one expects from [4], the same equation, together with Eq. (3.13), shows that positive characteristic slope also makes wave amplitude grow.

The most interesting question for these equations to answer is that posed in the INTRODUCTION, namely, how the known resonance properties of the linear solution come into play during nonlinear transients. The section to follow will focus on this issue.

4. TRANSIENT SOLUTIONS

Singularities of Linear Solution

Ref. [1] showed how $\hat{A}$, $\hat{B}$, and $\hat{PR}$ have singularities as functions of flow coefficient Φ. It can easily be shown that these singularities are all simple poles in general. For the present purpose of illustration, a particular case will be considered that is easily analyzed, namely parallel walls (n = 0), $r_F = 2.08$, and the fundamental mode (b = 1), for which Fig. 1.2 suggests that propagation speed f vanishes at the resonant condition, $\Phi^* = 0.15464$. (Asterisks will denote the resonant, or singular condition.) As flow coefficient is changed, the value of f will also change, but as Fig. 1.2 illustrates, f is minimum at resonance. Thus it is surely accurate to assume f constant when Φ is near Φ^*.

For the particular case defined above,

$$f = 0\,; \quad n = 0; \quad b = 1 \tag{4.1}$$

the solution of Eqs. (9 through 11) of [1] can be written, in notation of [1],

$$A = \alpha\, r^{1-\, i/\Phi} + \beta r^{-2} + \gamma \tag{4.2}$$

$$w = i\left[\alpha\left(2 - \frac{i}{\Phi}\right) r^{1\,-\, i/\Phi} - \beta r^{-2} + \gamma\right] \tag{4.3}$$

$$rP = -2\Phi\alpha\left(2 - \frac{i}{\Phi}\right) r^{1-\, i/\Phi} + (i - \Phi)\,\beta r^{-2} - (i + \Phi)\,\gamma \tag{4.4}$$

The boundary conditions

$$A(1) = 1\ ; \quad W(1) = 0\ ; \quad P\,(r_F) = 0 \tag{4.5}$$

allow β and γ to be expressed in terms of α , and provide the real and imaginary parts of α as follows:

$$\alpha_{real} = \frac{G}{G^2+M^2}\,\Phi\,(1+ r_F^{-2}) + \frac{M}{G^2+M^2}\,(1- r_F^{-2}) \tag{4.6}$$

$$\alpha_{imag} = \frac{G}{G^2+M^2}\,\Phi\,(1-r_F^{-2}) + \frac{M}{G^2+M^2}\,\Phi\,(1+r_F^{-2}) \tag{4.7}$$

where these definitions apply:

$$\vartheta = -\frac{\ln r_F}{\Phi} \tag{4.8}$$

$$G = -4r_F \sin\vartheta - 8\,\Phi r_F \cos\vartheta + \frac{1-\Phi^2}{\Phi r_F^2} + \frac{1+3\Phi^2}{\Phi} \tag{4.9}$$

$$M = 4r_F \cos\vartheta - 8\,\Phi r_F \sin\vartheta + 2\,(1+r_F^{-2}) \tag{4.10}$$

Eqs. (4.6) and (4.7) indicate that there is a singularity only when G and M vanish separately, and solving Eqs. (4.9) and (4.10) gives the conditions

$$\cos\vartheta^* = \frac{(3\,r_F^2-1)\,\Phi^{*2}}{2(1+4\Phi^{*2})r_F^3} \tag{4.11}$$

$$\sin\vartheta^* = \frac{1+r_F^2+\Phi^{*2}\,(3+7r_F^2)}{4\Phi^* r_F^3(1+4\Phi^{*2})} \tag{4.12}$$

which in turn can be solved to discover that, for this case (Eq. (4.1), resonance occurs at

$$\Phi^* = 0.15464 \quad \text{if} \quad r_F = 2.08 \tag{4.13}$$

The singularity is clearly a simple pole, and one may use the foregoing results in Eq. (4.4) to find the real part of the pressure singularity, needed for Eq. (2.43). Because G and M vanish there, derivatives with respect to Φ^* will appear:

$$G'(\Phi^*) = -4\, r_F \left[\left(-\frac{\vartheta^*}{\Phi^*} + 2\right)\cos\vartheta^* - 2\Phi^*\left(-\frac{\vartheta^*}{\Phi^*}\right)\sin\vartheta^*\right.$$

$$\left. - \frac{1}{\Phi^{*2}\, r_F^2}\left[1 + \Phi^{*2} + (1-3\Phi^{*2})\, r_F^2\right]\right. \tag{4.14}$$

$$M'(\Phi^*) = -4 r_F \left[\left(-\frac{\vartheta^*}{\Phi^*} + 2\right)\sin\vartheta^* + 2\Phi^*\left(-\frac{\vartheta^*}{\Phi^*}\right)\cos\vartheta^*\right] \tag{4.15}$$

In present notation, then, the pressure singularity is

$$\hat{P}R_1 = \frac{1}{\Phi-\Phi^*}\,\frac{1}{G'^2+M'^2}\left\{G'\left[(1-3\Phi^{*2})\,(1+r_F^{-2}) - 4\,(1-r_F^{-2})\right]\right.$$

$$\left. + \frac{M'}{\Phi^*}\left[(1-3\Phi^{*2})\,(1-r_F^{-2}) + 4\Phi^{*2}\,(1+r_F^{-2})\right]\right\} \tag{4.16}$$

It is necessary also to find the singularity of the integral in Eq. (2.42):

$$I = \int_1^{r_F} \left[r(\hat{A}_r^2 + \hat{B}_r^2) + \frac{2}{\Phi}(\hat{B}\,\hat{A}_r - \hat{A}\,\hat{B}_r)\right]dr \tag{4.17}$$

After arduous but straightforward analysis, one finds the result:

$$I = \frac{1}{(\Phi-\Phi^*)^2}\left[\frac{\Phi^{*2}\,(1+r_F^{-2})^2 + (1-r_F^{-2})^2}{L'^2 + M'^2}\right]\left\{\left[-\frac{1}{2}\, r_F^2\left(\frac{1}{\Phi^{*2}} - 1\right) + \right.\right.$$

$$\left.\frac{1}{4}(1+r_F^{-2})\left(1+\frac{1}{\Phi^{*2}}\right) - \frac{1}{\Phi^{*2}}\right](1-r_F^{-2}) + \left[\frac{2}{r_F} - \frac{1}{\Phi^{*2}}\left(r_F - \frac{1}{r_F}\right)\right]\cos\vartheta^*$$

$$\left. -2 - \frac{1}{\Phi^*}\left(3r_F + \frac{1}{r_F}\right)\sin\vartheta^*\right\} \tag{4.18}$$

This quantity, it should be noted, is a second-order pole.

Inserting Eq. (4.13) into Eqs. (4.16) and (4.18) gives numerical values for pole strengths in this particular case: (For simplicity, Φ will hereafter be measured from the appropriate critical value; that is, $\Phi^* = 0$.)

$$\hat{PR}_1 = - b^* \frac{m + \frac{1}{2a}}{2l_c} \frac{1}{\Phi}; \quad \text{where } b^* = 0.020166 \frac{2l_c}{m + \frac{1}{2a}} \tag{4.19}$$

$$I = -2c^* \frac{1}{\Phi^2}; \quad \text{where } c^* = 0.0005062 \tag{4.20}$$

Simplified Example Near Resonance

Reduction of equations. It is now possible to illustrate the behavior of the transient equations (3.42, 3.43 and 3.44) near the resonant point for $r_F = 2.08$ (chosen for the analytic simplicity which results). Only the singular parts of the coefficients of Φ need be kept. Also, because the focus is to be on the effect of resonance, the characteristic function $\psi_c(\Phi)$ will be assumed locally to have a constant slope SL. Zero slope would imply neutral damping for disturbances. Arbitrarily, one may then choose $\psi_c(0) = 0$, and also measure flow coefficient from the resonant value. The three transient equations then reduce to

$$\Psi - SL\,\Phi + l_c\,\Phi_\xi + c^* \frac{J}{\Phi^2} = 0 \tag{4.21}$$

$$l_c\,J_\xi - b^* \frac{J}{\Phi} = 0 \tag{4.22}$$

$$l_c\,\Psi_\xi - \frac{1}{4B_g^2}(\Phi - \Phi_T) = 0 \tag{4.23}$$

These equations can further be simplified in appearance by making the following scaling transformations:

$$\Phi = 2B_g b^* q \tag{4.24}$$

$$\Psi = b^* z \tag{4.25}$$

$$J = \frac{4B_g^2 b^{*3}}{c^*} \lambda \tag{4.26}$$

$$\xi \equiv 2B_g l_c\,\zeta \tag{4.27}$$

$$SL \equiv \sigma/2B_g \tag{4.28}$$

so that the three governing equations become

$$z - \sigma q + q\,\zeta + \frac{\lambda}{q^2} = 0 \tag{4.29}$$

$$\lambda_\zeta - \frac{\lambda}{q} = 0 \tag{4.30}$$

$$z_\zeta - (q - q_T) = 0 \tag{4.31}$$

At $\zeta = 0$, initial values of the quantities z, λ, and q (which must be near 0, of course) would be specified, and then would be caused or allowed to change, perhaps under influence of the throttle coefficient q_T.

Small perturbations. Because q must be and remain small for the governing equations to be valid, it seems reasonable to further transform variables to reflect a small initial value of flow-coefficient disturbance, ε:

$$q = \varepsilon Q \;\; ; \;\; z = \varepsilon Z \;\; ; \;\; \lambda = \varepsilon^2 L \tag{4.32}$$

The governing equations now are

$$\varepsilon Z - \varepsilon\sigma Q + \varepsilon Q_\zeta + \frac{L}{Q^2} = 0 \tag{4.33}$$

$$\varepsilon L_\zeta - \frac{L}{Q} = 0 \tag{4.34}$$

$$Z_\zeta - (Q - Q_T) = 0 \tag{4.35}$$

with initial conditions

$$Q(0) = 1 \;\; ; \;\; L(0) = L_o \;\; ; \;\; Z(0) = 0 \;\; ; \;\; Q_T(0) = Q_{T_0} \tag{4.36}$$

It is necessary to specify an initial rotating-wave disturbance level (L_0), which might arise from inlet distortion or some similar cause.

Although ε may be considered much less than 1, the equations do not thereby become linear, because of the singularities. However, the equations may be expanded in powers of ε, and "inner" and "outer" solutions may be identified. These solutions will be identified and discussed, and then related numerical solutions will be presented.

Inner and outer solutions. The appropriate "inner" variable is

$$\zeta' \equiv \zeta/\varepsilon \tag{4.37}$$

and when this variable is used, the inner small-ε solution proves to be

$$Z = 0 \tag{4.38}$$

$$\frac{Q}{k} + \frac{1}{2} ln \left| \frac{Q-k}{Q+k} \right| = \frac{1}{2} \frac{\zeta'}{k} \tag{4.39}$$

$$L = \frac{1}{2} (k^2 - Q^2) \tag{4.40}$$

where k is a constant related to the initial value of L :

$$k^2 = 1 + 2 L_0 \tag{4.41}$$

The flow coefficient Q defined by Eq. (4.39) and the corresponding rotating-wave amplitude L defined by Eq. (4.40) are displayed on Fig. 4.1.

This inner solution provides the most significant result of this paper, that flow coefficient cannot decrease smoothly through a resonance value of Φ. Rather, an abrupt drop must occur, to a level just as far below resonance as it was above resonance when the transient began. During this drop, rotating-wave amplitude increases to a finite maximum level

$$L_{max} = \frac{1}{2} k^2 = \frac{1}{2} + L_0 \tag{4.42}$$

and and then decreases. It is noteworthy that this increase is limited to a value of 0.5 above the initial level.

The beginning of the process just described can be imagined to occur as the result of a reduction of throttle flow Φ_T, which brings Φ into the range of negative damping; above that level, the terms involving L would not

appear. Fig. 1.2 shows that amplification begins, for the case of present interest, when Φ is about 0.01 above resonance. Consulting Eqs. (4.24) and (4.32), and assuming that B_g is about 1 and l_c is about 10, one finds that the choice $\varepsilon = 0.01$ places the beginning of the transient ($Q = 1$) at the beginning of amplification. That is the value to be used subsequently. It is interesting that neither the characteristic slope nor the throttle schedule have any influence on the abrupt, "inner" process.

The influence of initial wave amplitude L_0 may be inferred from Eq. (4.39) or Fig. 4.1. Especially, the limit as L_0 vanishes is of interest. In that limit, k approaches 1, and the initial conditions $Q = 1$ and $Q = 0$ will be met only at $\zeta' = -\infty$, on the "inner" scale. This reasonable result means that if the initial wave amplitude is very small, then the time for the wave to grow will be very long, but only on the short time scale of the drop to follow.

One may question why the singular solution goes only one way; why an increase of Φ is not allowed. Apparently, Φ can increase smoothly through resonance because it approaches resonance through values of Φ for which the relevant wave is strongly damped. Then as it reaches values above resonance, the amplification has no wave amplitude to amplify, and the amplitude may remain zero as Φ continues to increase.

The "inner" time scale is very short; if $\varepsilon = 0.01$, shorter by a factor of 100 than the "outer" scale which is based on ζ itself. The outer solution does depend on the throttle and the characteristic slope; if one is held constant and the other set equal to zero, the leading outer approximation is simply a harmonic surge wave with an amplitude matched to the final (negative) inner limit for Q, with no rotating-wave amplitude, and with phase determined by matching to the inner value of Z at $\zeta = 0$:

$$L = 0 \tag{4.43}$$

$$Q = Q_T - (Q_T + k)\cos\zeta \tag{4.44}$$

$$Z = -(Q_T + k)\sin\zeta \tag{4.45}$$

Further consideration of matching shows that, to leading order, the outer and inner solutions have the same origin, namely where Q crosses resonance. To first order in ε, a phase shift would apply in the outer solution.

Thus, a surge transient must follow the sudden drop at resonance, triggered by that drop. The subsequent course of the surge transient naturally depends on the throttle schedule and the characteristic slope. In principle, however, at any subsequent time when the surge transient carries downward through resonance, another sudden change with rotating-wave features could occur.

Numerical Solutions

Eqs. (4.33 through 4.36) can easily be solved numerically, of course, and a number of such solutions for various parameter choices will next be described. The foregoing theoretical results show that the "inner", abrupt changes will depend only on initial conditions of Q and (slightly) L. The throttle schedule and characteristic slope will have effect only on the "outer" scale; therefore, the figures will present results on that scale (ζ).

Slow throttle closure. Fig. 4.2 shows results (on the "outer" scale) of a numerical solution of Eqs. (4.33 through 4.36), for the indicated parameter choices, which correspond closely to the theoretical results just discussed. Amplification was assumed to occur only in the range $1< Q < 0$, and damping only in the range $0 < Q < -4$, as Fig. 1.2 implies. The essential action indicated on Fig. 4.2 results from a slow throttle closure (K_1) from an initial level (K_0), just above the amplification range, where both Q and Q_T agree.

$$Q_T \equiv K_0 - K_1 \zeta \tag{4.46}$$

The results illustrate the "inner and outer" solutions; the flow coefficient slowly descends, and pressure-rise function Z slowly rises, in response to Q_T, until the amplification range is entered at $Q = 1$. Then a sudden drop (Eq. (4.39)) occurs, together with a burst of rotating-wave amplitude (L). Following that drop, a surge process begins and continues indefinitely (The characteristic slope σ is zero in this example.)

As anticipated in the discussion of the "inner" solution, the effect of changing initial wave amplitude L_0 from 0.1 to 0.01 is indistinguishable on the scale of Fig. 4.1, except for the level of L between $\zeta = 0$ and 2, where the drop appears.

One sees that when Q passes through zero again, at about $\zeta = 7$, another sudden drop occurs, with a reappearance of rotating-wave amplitude L. The reason for this event is that, following the first drop (at about $\zeta = 2$),

Q is negative, and the rotating wave is damped exponentially to a very small amplitude; but then the surge effect provides enough re-amplification (between ζ about 3 to 7), so that a non-zero resonance occurs when Q passes down through the axis again. This second "inner" type of wave is weaker than the first because the corresponding velocity drop is weaker, as Eq. (4.40) implies.

It should be emphasized that the strength of the surge oscillation shown in Fig. 4.2 is due to the resonance. Fig. 4.3 shows how the transient would develop if there were no resonance effect at all. (In the calculations, L was held equal to zero.) A very weak surge is indicated, as flow coefficient follows the changing throttle coefficient.

Effect of throttle closure rate. Figs. 4.4 and 4.5 show the corresponding results if the transient begins at a much higher flow coefficient, and the throttle closure is much faster. Qualitatively, the results are the same for the surge effect, and the resonant drop is quantitatively the same, as expected, because it depends only on conditions existing just when resonance occurs.

Figs. 4.6 and 4.7 show results when the throttle is abruptly closed at ζ= 0, to a level calling for a change of flow coefficient from 1.1 to -1.1, which is below the resonant value. Fig. 4.6 shows that, again, a surge develops after the sudden transition, but there is no second resonance, because the surge does not penetrate into the amplifying range of Q between 0 and 1. Fig. 4.7 shows the contrasting result if the rotating wave L is suppressed. In this case, the surge is stronger. In effect, resonance gives a weaker surge because the sudden drop happens to place Q close to the level demanded by the new throttle setting anyway.

Fig. 4.8 shows what happens when the throttle is abruptly closed again from 1.1, but only to 0. As might be expected, after the first sudden drop, the flow coefficient hunts around the resonant value, with an indefinite succession of weak resonant transitions.

Effect of characteristic slope. Next, the effect of characteristic slope (σ) is considered. One expects that positive values will lead to amplification of surge, and perhaps of rotating waves as well; negative values typically damp surge, and they certainly suppress rotating stall in axial machines. So far, only the neutral situation ($\sigma = 0$) has been discussed.

First, a small positive (destabilizing) slope of $\sigma = 0.2$ is considered, with a slow throttle closure. The result, shown in Fig. 4.9, may be compared

with Fig. 4.2, for which $\sigma = 0$. The result is similar, except that the surge induced be the resonance is amplified, as expected. Also, there seems to be no secondary resonance, presumably because the rotating-wave damping is so strong.

Fig. 4.10 then shows the result when the characteristic slope is negative. The surge motion is indeed damped as one expects, but secondary resonance events of some strength appear. If the slope is more strongly negative, as in Fig. 4.11, this tendency is accentuated; a succession of resonant transitions occur which are about as strong as the first one, and they occur in rapid succession. The flow coefficient shows a saw-tooth pattern with time; a sort of "stick-slip" oscillation about the throttle value. The pressure-rise coefficient (Z) drifts toward negative values, which is opposite to the trend expected when the throttle closes and the characteristic slope is negative. Fig. 4.11 may be contrasted with Fig. 4.12 which is the same except that rotating waves are suppressed. In the latter case, surge-like waves are weak, and the pressure rise ultimately begins to rise in response to the throttle. Clearly, resonance is predicted to produce a dramatically different transient behavior, even when on the "stable" slope of the characteristic.

The successive surge transients shown in Fig. 4.11 continue until the peaks of Q become negative; then the rotating waves are no longer amplified. Fig. 4.13 illustrates this effect for a higher throttle closure rate. After about $\zeta = 5$, the resonance no longer operates, because Q stays below 1. Subsequently, Q follows the throttle more closely, and Z steadily increases as the characteristic slope requires.

Finally, a still steeper "stable" slope of $\sigma = 1$ gives the results of Fig. 4.14, in which the tendencies just described are accentuated.

Resonant capture of surge. If a surge transient occurs about a throttle setting which is above the range of amplification, and the surge happens to carry Q into the amplification range, the sigularity "captures" the oscillation. Figs 4.15, 4.16, and 4.17 show this effect, for a strongly stable $\sigma = 1$. The throttle is set for 1.1, 1.4, and 2.4, respectively. In each case, begins at 2.0. Fig. 4.15 shows successive capture, which presumably recurs indefinitely; Fig. 4.16 shows capture, but insufficient time in the amplification range for recurrence; Fig. 4.17 shows a case with the throttle setting so high that the amplification range is not entered at all, and there is no capture.

Resonance for Higher Harmonics

Fig. 1.2 was the basis for the foregoing analysis, and it concerned the first circumferential harmonic for a traveling wave. The singularity was associated with the lower branch of the wave-speed (f) versus flow coefficient (Q) function, and f would be quite stationary at zero, near the singularity, for the particular case chosen for study. Actually, as explained in [1], the third or fourth harmonics are more technically interesting; they would be found at higher flow coefficient according to both theory and experiment.

The shape of the amplification curve for the third harmonic, for example, is different from that shown in Fig. 1.2; Fig. 2.2 suggests that the function f(Q) has a cusp at the singular point, and that amplification occurs for the upper branch of that function. There is virtually no damping on that branch; damping is associated with a slightly lower wave speed. Unfortunately, there is no easy way to evaluate singularity strengths in this case, because the simplification of $f = 0$ is not available for any reasonable set of parameters. Nevertheless, one may speculate that equations similar to Eqs. (4.33) through (4.35) would still apply, after certain changes are made: For negative Q, amplification is positive; therefore, the sign of the L/Q term of Eq. (4.34) is changed. It is assumed that the last term of Eq. (4.33) remains as written, because it depends on the square of Q. Further, it is imagined that both those terms apply only when Q is between 0 and -4; otherwise, they are both taken to be zero.

The solution of the revised equations is quite different from the previous one. The "inner" solution

$$Q = -\frac{1}{2}\zeta' \; ; \quad Z = 0 \; ; \quad L = \frac{1}{8}\zeta'^2 \tag{4.47}$$

applies even with no initial value of L. The maximum L is 8, whereas it was only 0.5 in the previous case. Also, because there is no damping, wave amplitude remains high even though Q may pass below the range of amplification; previously, L would return to zero. Fig. 4.18 shows a numerical calculation, on the "inner" scale, for the response to a sudden drop of throttle flow.

Fig. 4.19 follows the response on the long-term scale (Fig. 4.6 shows a comparable previous case.) Following the initial transient, a surge develops as before, but now the wave amplitude does not return to zero; in fact, the next time the surge comes to $Q = -1$, a new increment of L appears. As one

would expect, if the characteristic slope is even slightly positive (destabilizing for surge), this effect is accentuated (Fig. 4.20), and with each surge cycle, the traveling wave would be kicked to a considerably higher level. If the slope were negative, no such kick would occur, and L would stay at the level of 8.

5. TRANSIENTS WITH MULTIPLE ROTATING MODES

Away from resonant conditions, the possibility of more than one wave type should be considered, because two families of rotating waves (fast and slow) are in principle allowed. Furthermore, many different slow-wave modes could possibly coexist. That is, instead of Eqs. (3.10) and (3.11), one would begin with

$$g = W\,[A_1^{(1)}) \cos(\theta - f^{(1)}\xi) + A_1^{(2)}) \cos(\theta - f^{(2)}\xi) + \ldots] \tag{5.1}$$

$$P = \bar{P}\,(r,\xi) + {}_1P^{(1)}\cos(\theta - f^{(1)}\xi) + {}_2P^{(1)}\sin(\theta - f^{(1)}\xi) + {}_1P^{(2)}\cos(\theta - f^{(2)}\xi) + {}_2P^{(2)}\sin(\theta - f^{(2)}\xi) + \ldots \tag{5.2}$$

It seems clear that the Galerkin procedure can be applied only to angle variation, not time; the various modes are not orthogonal, and therefore averages over time cannot be defined. If appropriate expressions based on Eqs. (5.1) and (5.2) are introduced into Eq. (2.2), and then angle averages and the $\cos\theta$ and $\sin\theta$ moments are derived, a very complex set of unsteady equations result. They were not solved; however, they imply that one should expect surge-like beat pulsations depending on frequency differences, and one should expect some exchange effects between modes. These things would depend on products of amplitudes, of course, and would therefore be weak unless both component waves were quite strong.

It seems generally unlikely that two or more circumferential modes would be present in substantial strength at the same time. The various possible modes are subject to separate and different rates of amplification, often with resonance for some particular mode. Thus, it seems that one mode will almost always be singled out by the amplification process, and will predominate over the others.

For these reasons, the problem of multiple rotating modes is not pursued further in this report.

6. CONCLUSIONS

(1) The previous small-perturbation analysis of circumferential waves, assuming inviscid flow, does not depend on diffuser width; however, it does allow for radial convergence of the diffuser. Convergence confers stability in that the critical flow coefficient for the appearance of waves is reduced. The observation that narrow diffusers are more stable than wide ones is argued to be the result of boundary-layer displacement effect tending to make narrow diffusers relatively more convergent than wide ones.

(2) The Moore-Greitzer analysis for finite-strength transients containing both surge and rotating stall in axial machines can be adapted for the centrifugal compression system. In the axial case, the motivation was to explain "hung stall". In the centrifugal case, the motivation is to predict events when flow is throttled through resonance. As previously, a Galerkin procedure is adopted, and a cubic characteristic shape is assumed.

For a transient, it is assumed that wave speed is constant, that only squares of wave amplitude need be considered, and that flow in the diffuser, though time-dependent, is quasi-steady. These assumptions permit nonlinear expressions to be derived for pressure change and for a new, second-order swirl velocity. Except for this swirl, the diffuser velocity field can be carried over from the previous linear analysis.

The nonlinear equations confirm that negative values at the diffuser entrance of the coefficient of the pressure wave make the circumferential wave amplitude grow with time.

(3) The singularities of interest are simple poles in general. The pole strengths can be found analytically for a particular case of the fundamental mode and radius ratio of about 2; for that case, propagation speed happens to be zero.

Using the nonlinear transient equations, it is shown that throttling through a resonant value of flow coefficient cannot be smooth; flow coefficient must suddenly drop through that value in a surge-like transient, accompanied, of course, by a transient rotating wave. As in the axial analysis, it is necessary to postulate some pre-existing low initial level of circumferential disturbance, though the particular value chosen turns out not to be important.

A simple example shows this sudden drop to be an "inner" solution of the transient equations, while an "outer" solution on a longer time scale

governs the surge response to the initial excursion of flow coefficient. Typically, the long-term surge is much stronger than would be expected from throttle change alone. In fact, if throttle is set above the critical flow coefficient, the singularity may "capture" the flow, and a surge would occur purely as result of circumferential-wave resonance.

Numerical results are shown for various parametric choices relating to the throttle schedule and the characteristic slope. Especially interesting is the result of ramping through resonance when the characteristic slope happens to be negative; a rapid succession of surge excursions occur in a saw-tooth pattern.

(4) For higher circumferential modes, the simple pole type of singularity occupies a very narrow range of flow coefficient, and strong amplification seems to dominate for a range of flow coefficient beginning just below the critical. No analytical solution is available for such a case. However, it is suggested that the form of the result will involve strong surge oscillations, accompanied by rotating waves which do not die out, but rather accrete strength every time the surge passes through the resonant level.

(5) In principle, a number of circumferential modes should be considered simultaneously, because they all might be candidates to participate in a transient. It is shown how such a general Galerkin analysis would proceed, and it is expected that surge-like beat oscillations and mode-exchange effects could arise. However, it is argued that modes will probably appear separately because they are separately amplified, especially if resonance is involved. Thus, multiple circumferential modes are not treated further.

(6) To construct exact solutions of Eqs. (3.42)-(3.45), one would first establish a file corresponding to Figure 2.2, for example, including velocity and pressure profiles. That information would constitute the quasi-steady solution to be used as Φ varies. Eq. (3.45) would have been satisfied in forming that solution. Next, one would solve the remaining equations by marching in time; at each time step, the integral in Eq. (3.42) would be evaluated. Every time that Φ descends through a resonant point, the appropriate "inner" transition would be applied.

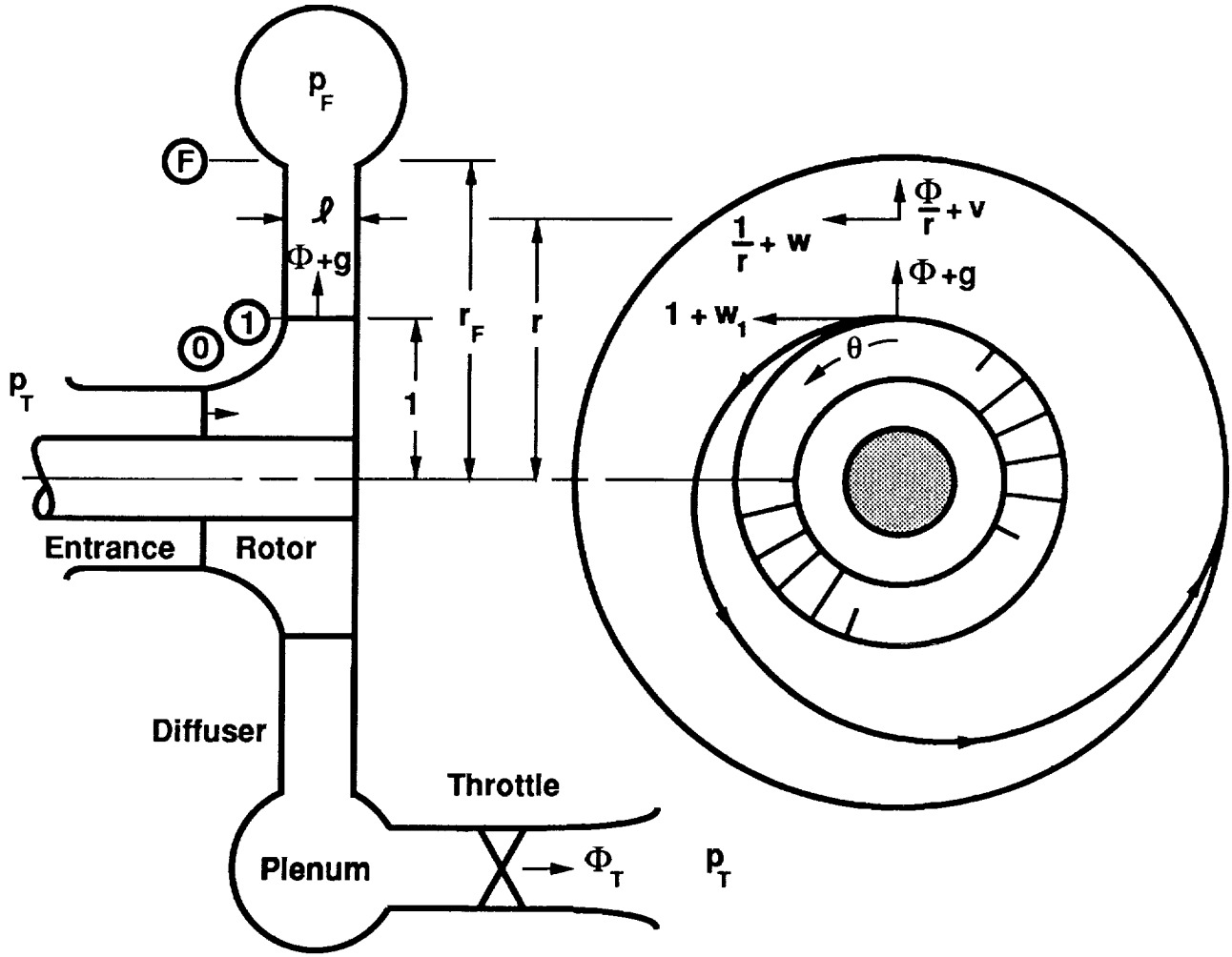

Fig. 1.1 Sketch of centrifugal compression system, schematically comprising entrance, rotor, diffuser, plenum, and throttled discharge.

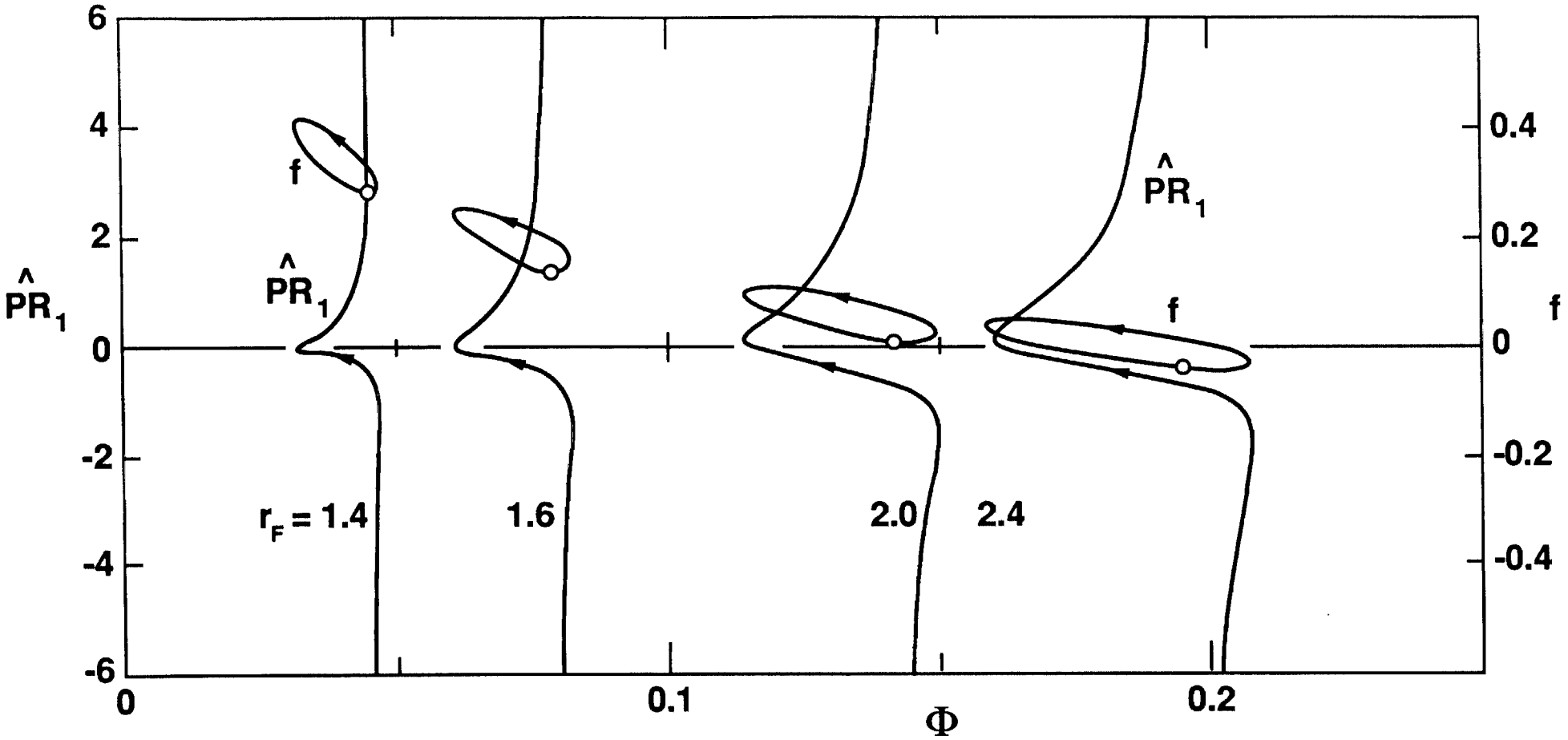

Figure 1.2 Amplification and wave speed for 1st mode (b=1), showing effect of radius ratio r_F. Negative values of $\hat{PR}_1$ signify amplification.

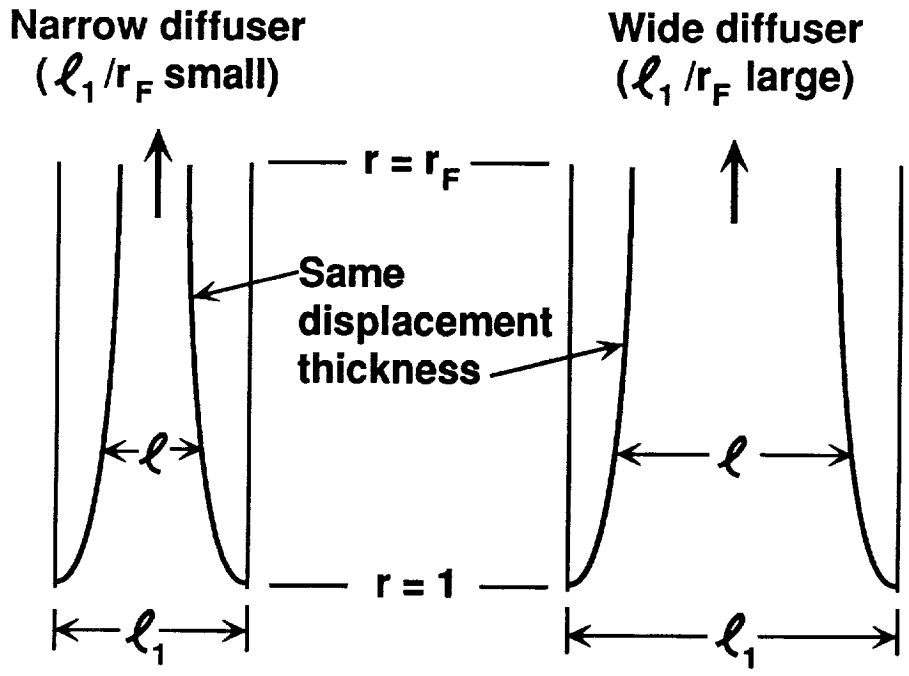

Figure 2.1 Sketch contrasting the boundary-layer displacement effect for a narrow and a wide diffuser.

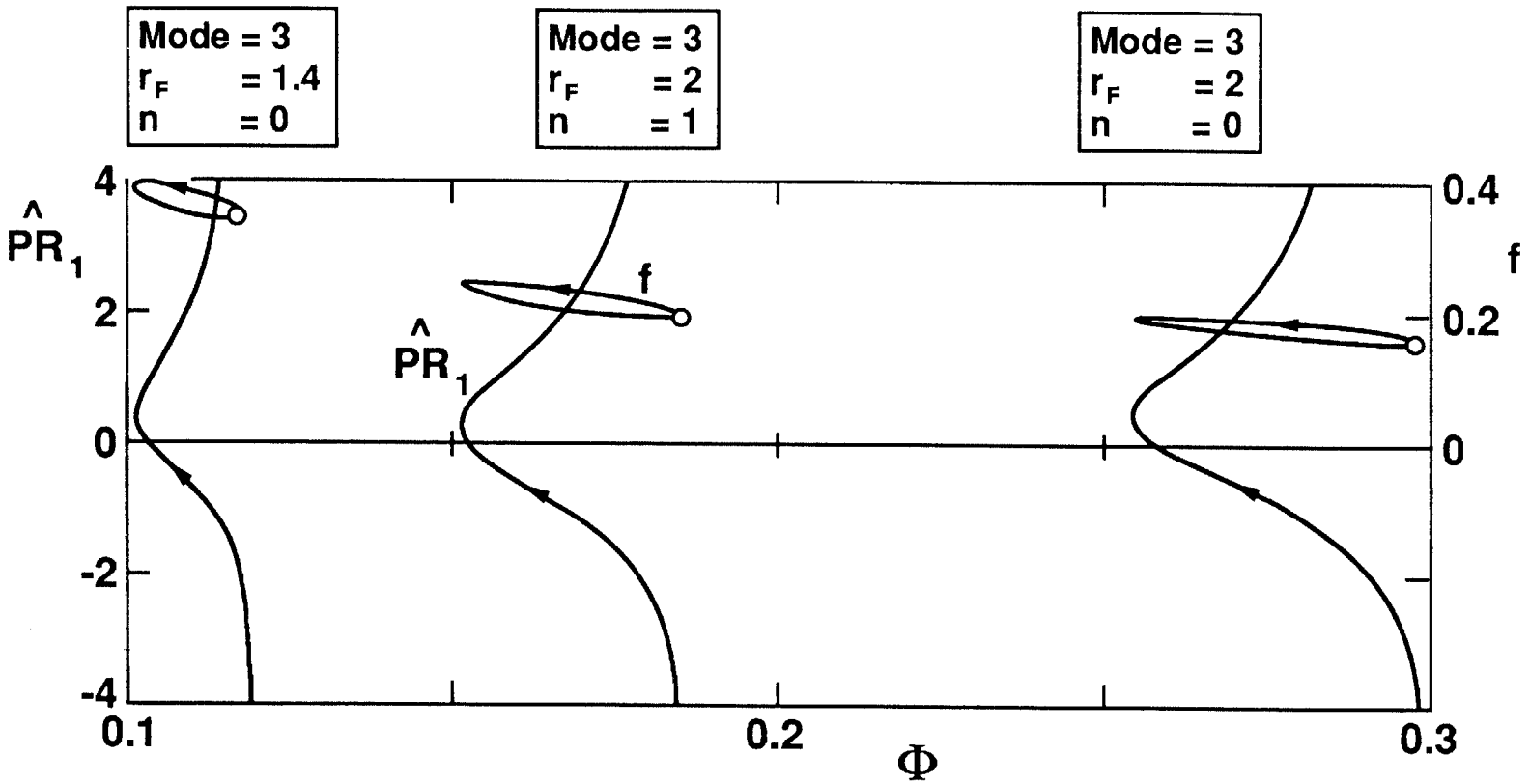

Figure 2.2 Amplification and wave speed for 3rd mode (b=3), showing effects of convergence (n) and radius ratio (r_F). Compare Figure 1.2. Negative values of $\hat{PR}_1$ signify amplification.

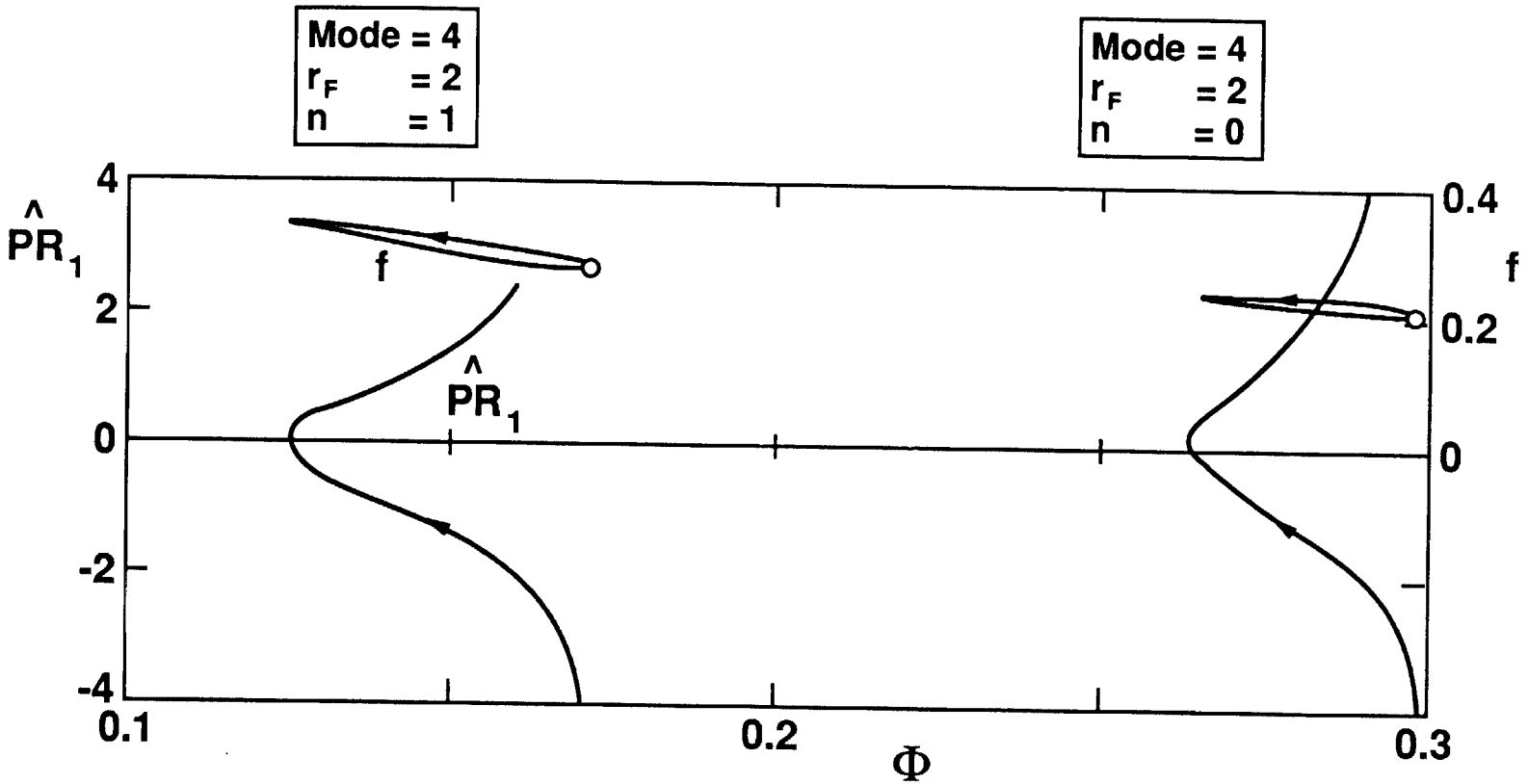

Figure 2.3 Amplification and wave speed for 4th mode (b=4), showing effects of convergence and radius ratio r_F. Negative values of $\hat{PR}_1$ signify amplification.

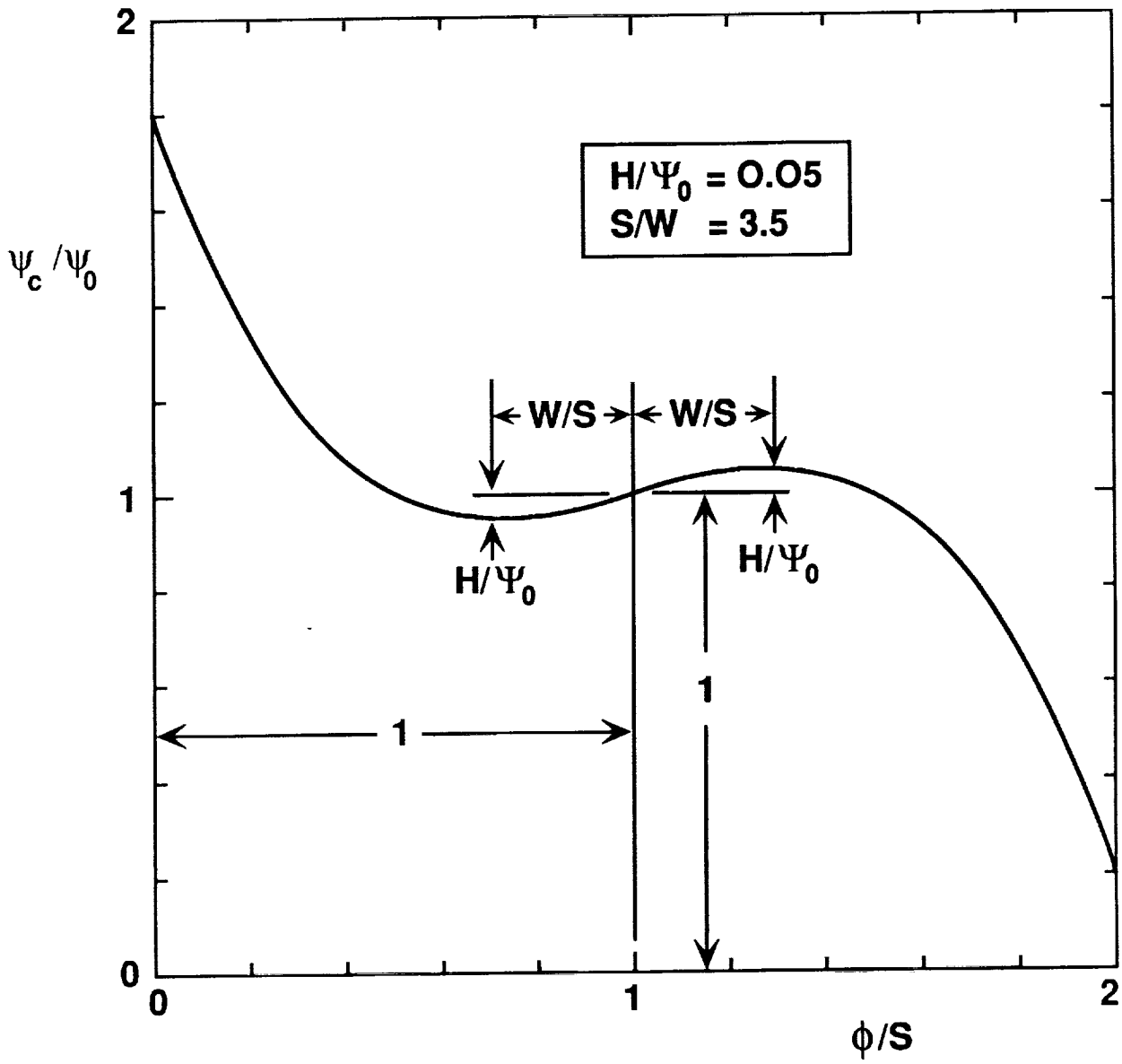

Figure 3.1 Postulated cubic axisymmetric compressor characteristic, shown for a particular set of the free parameters Ψ_0, H, W, and S.

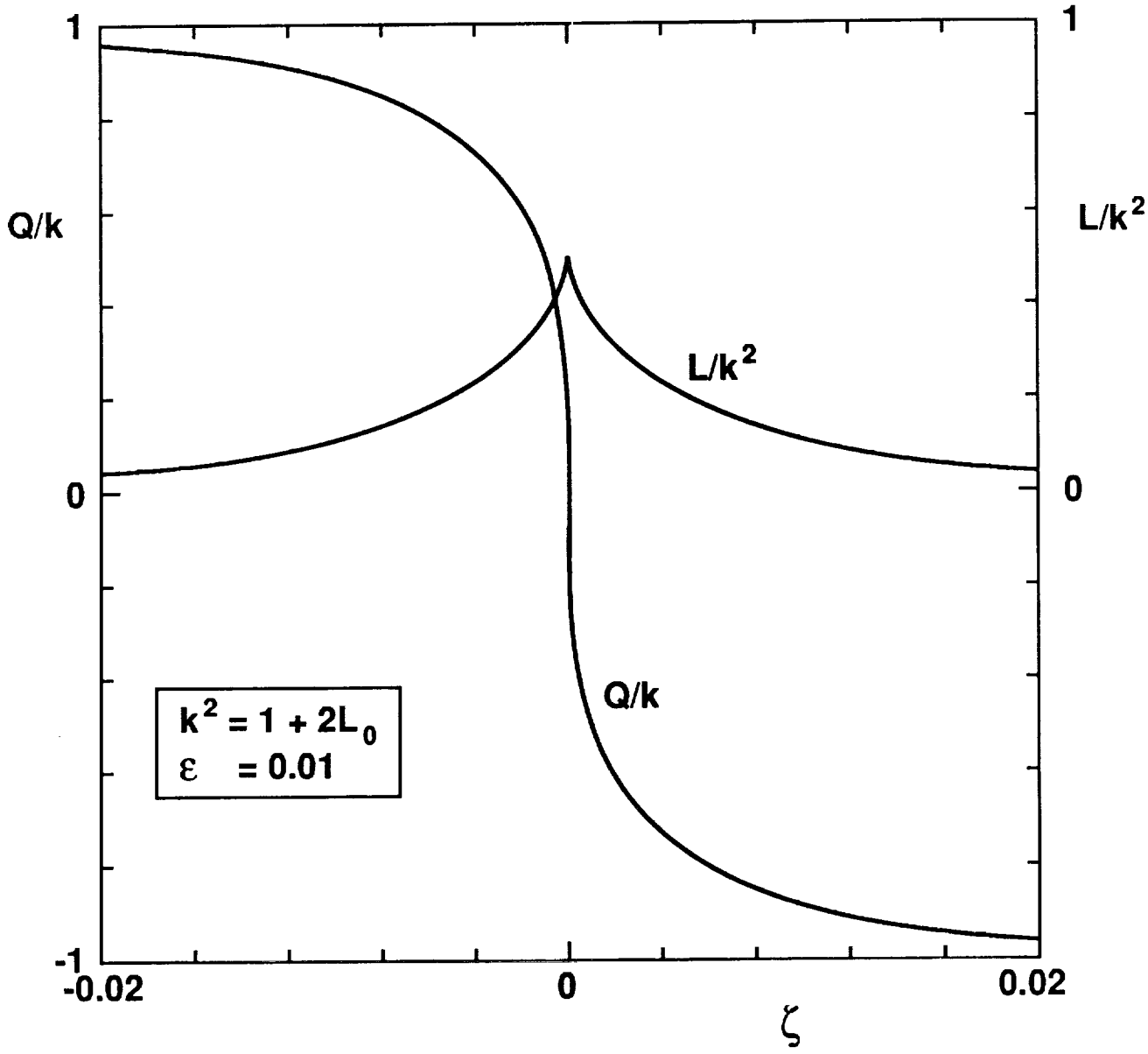

Figure 4.1 Inner solution for flow coefficient (Q) and square of wave amplitude (L), as functions of outer time variable (ζ).

Fig. 4.1 ART

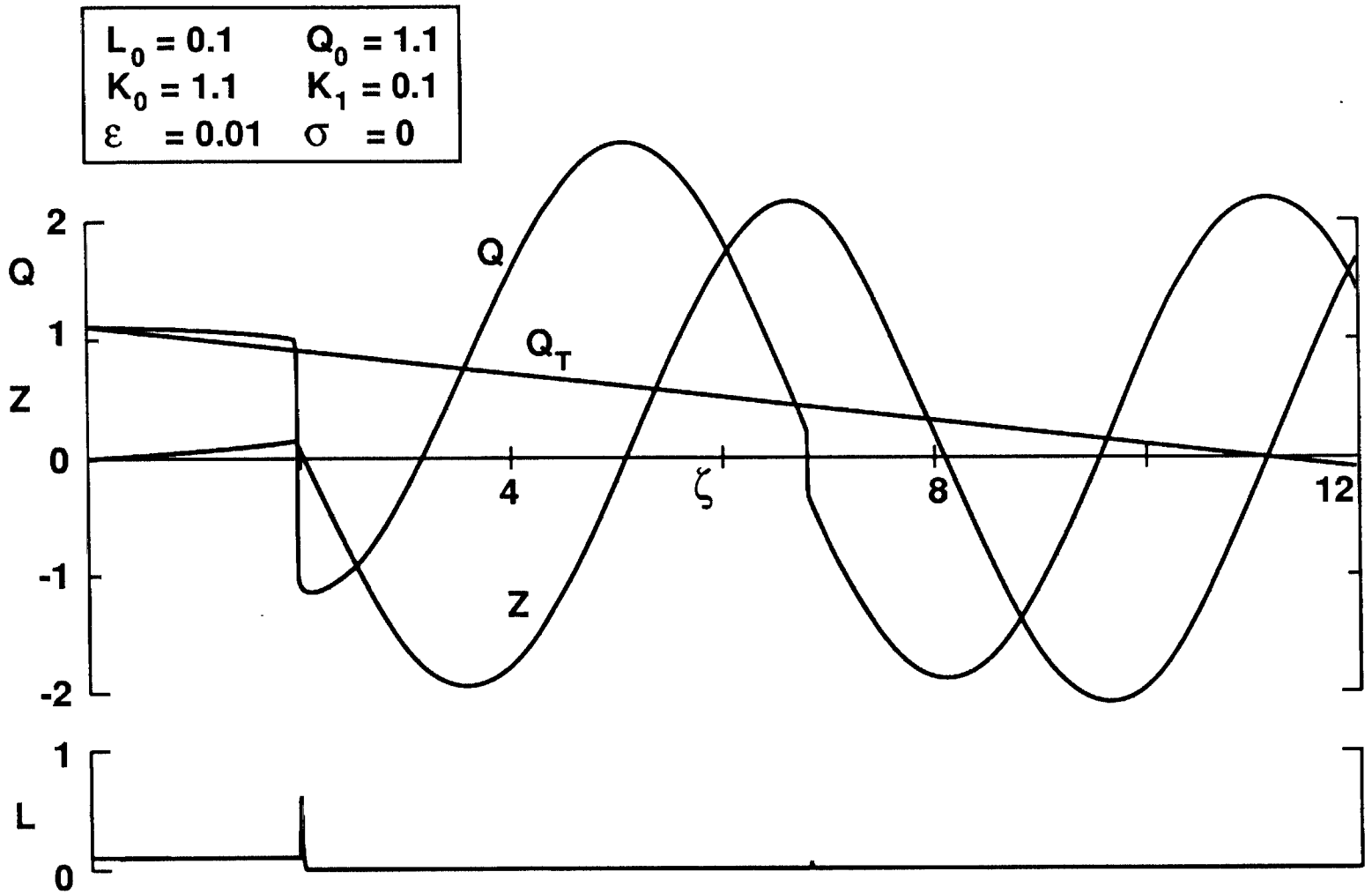

Figure 4.2 Solution for slowly closing throttle, showing surge oscillation following resonance occurring when ζ is about 2.

Fig. 4.2 ART

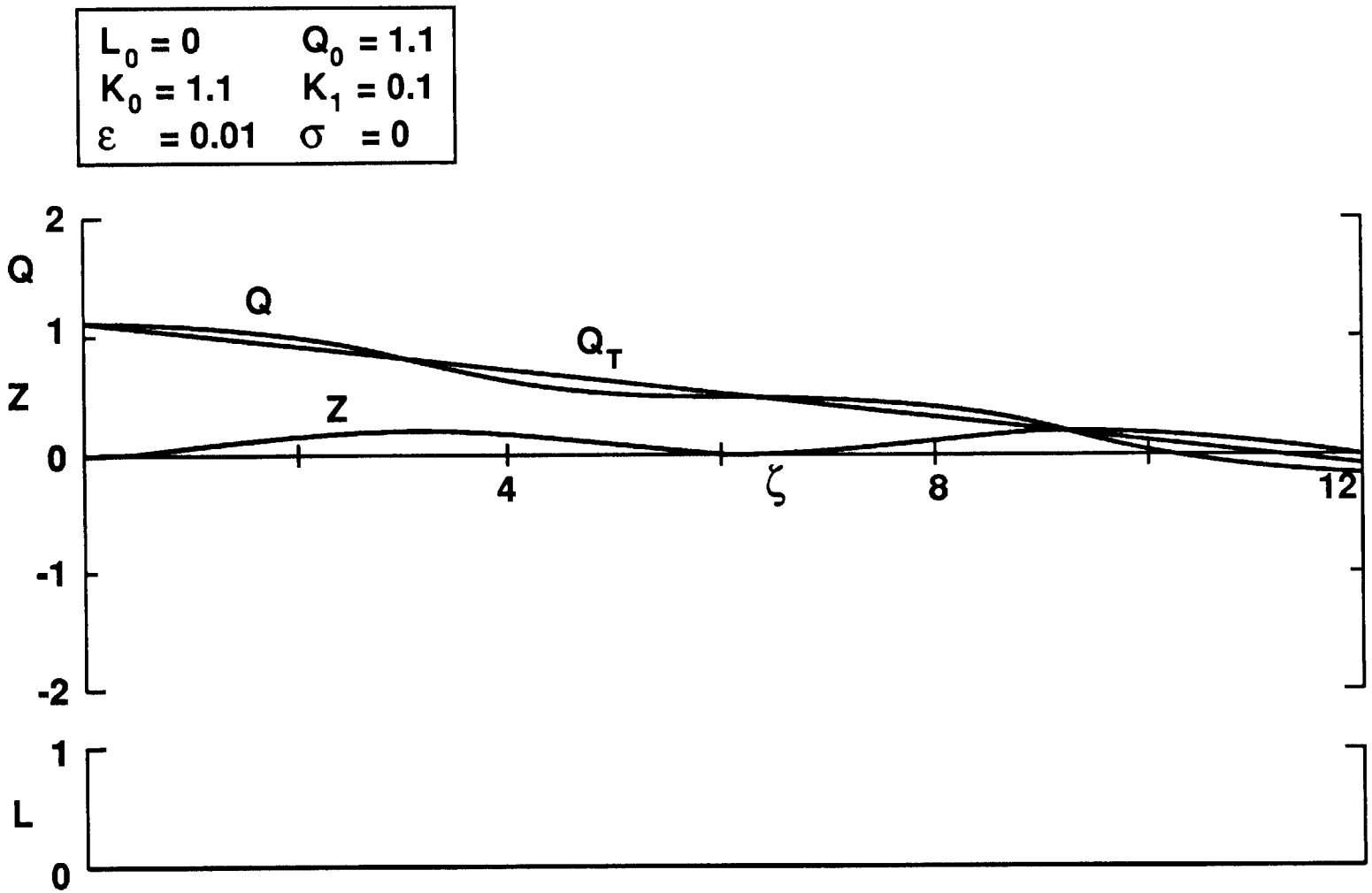

Figure 4.3 Solution for same conditions as previous Figure, except that resonance is suppressed by holding L = 0.

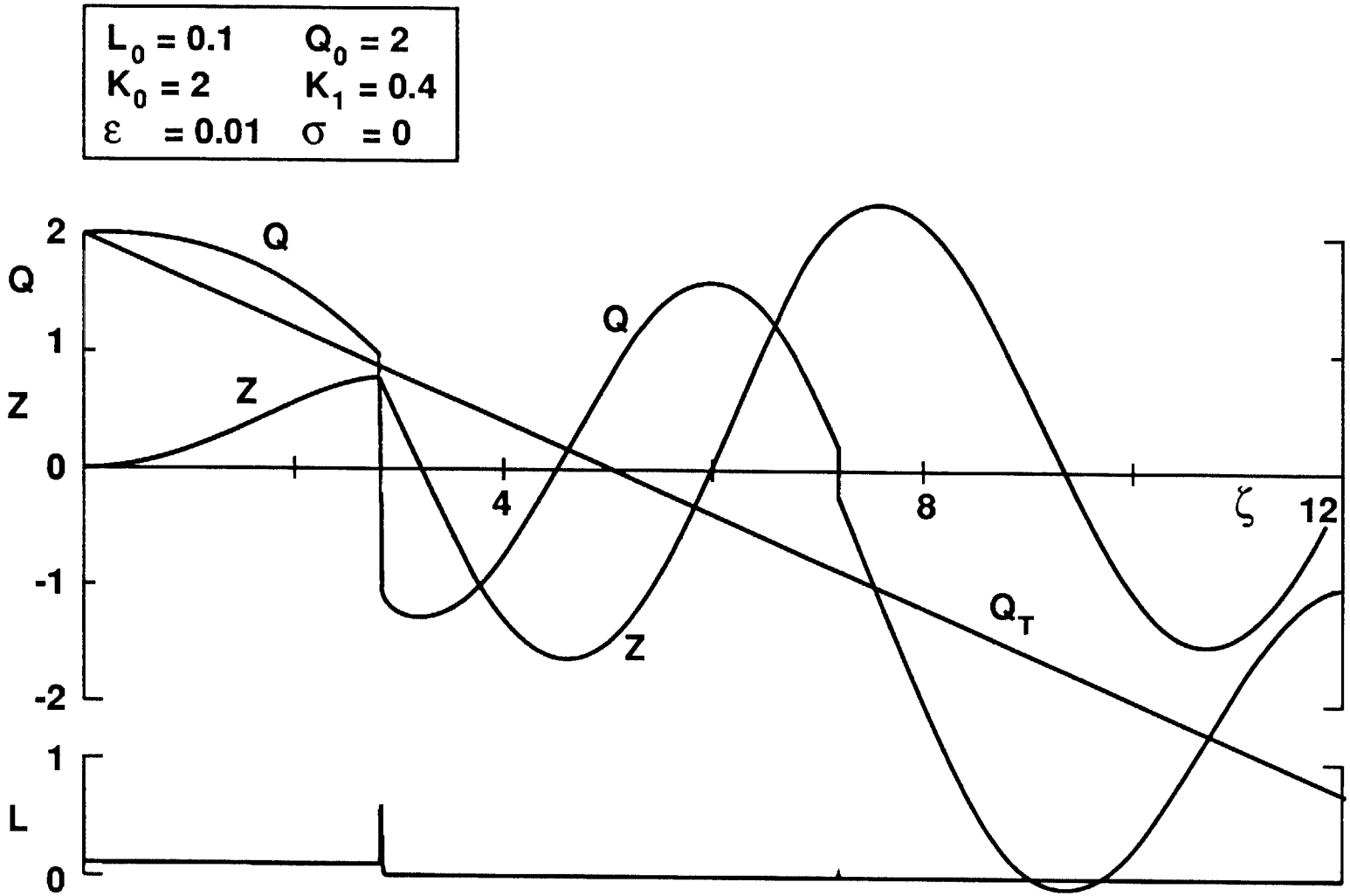

Figure 4.4 Effect of rapid throttle closure; otherwise same as Figure 4.2.

Fig. 4.4 ART

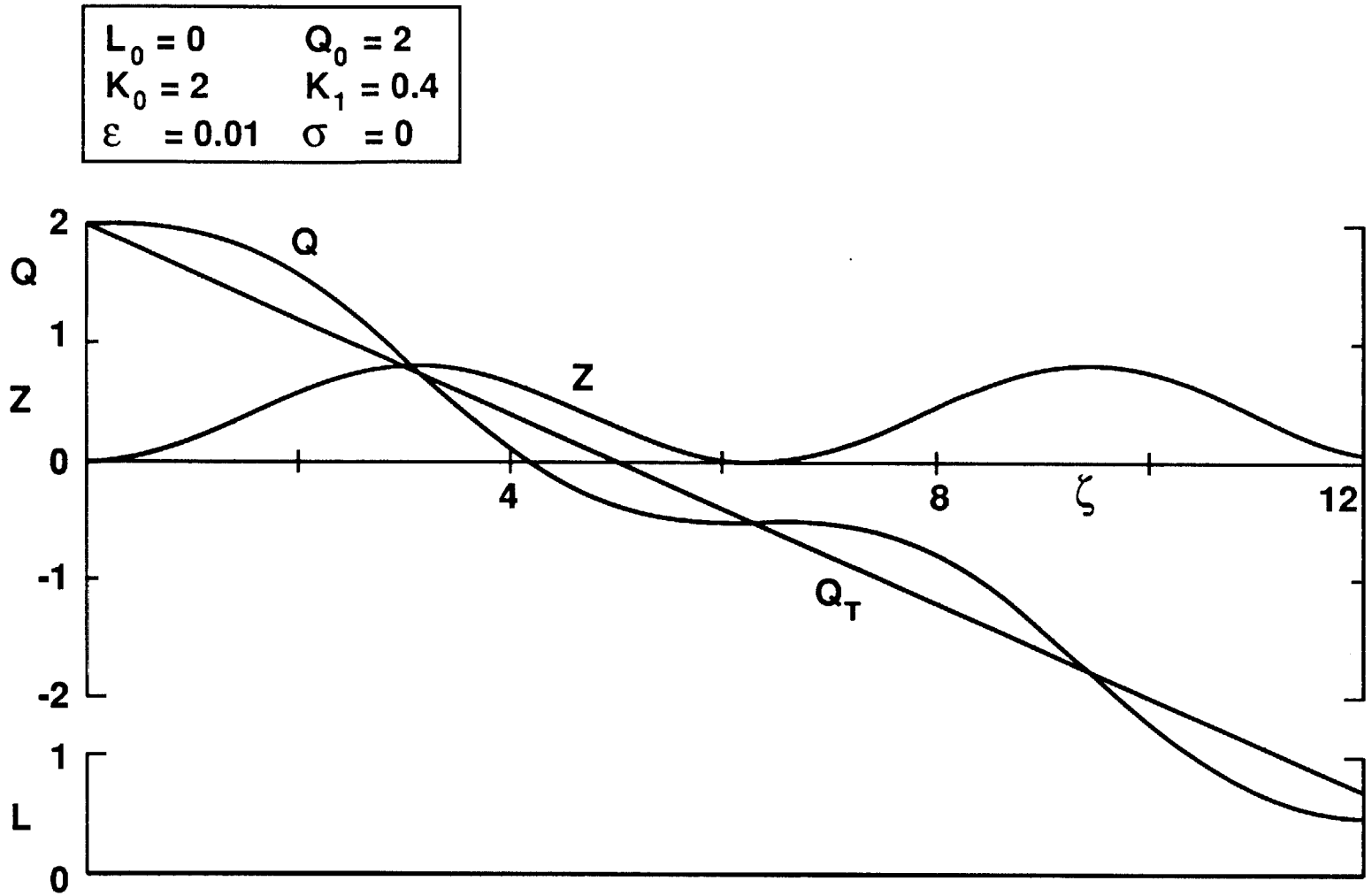

Figure 4.5 Same as previous Figure, except that resonance is suppressed by holding L= 0.

Fig. 4.5 ART

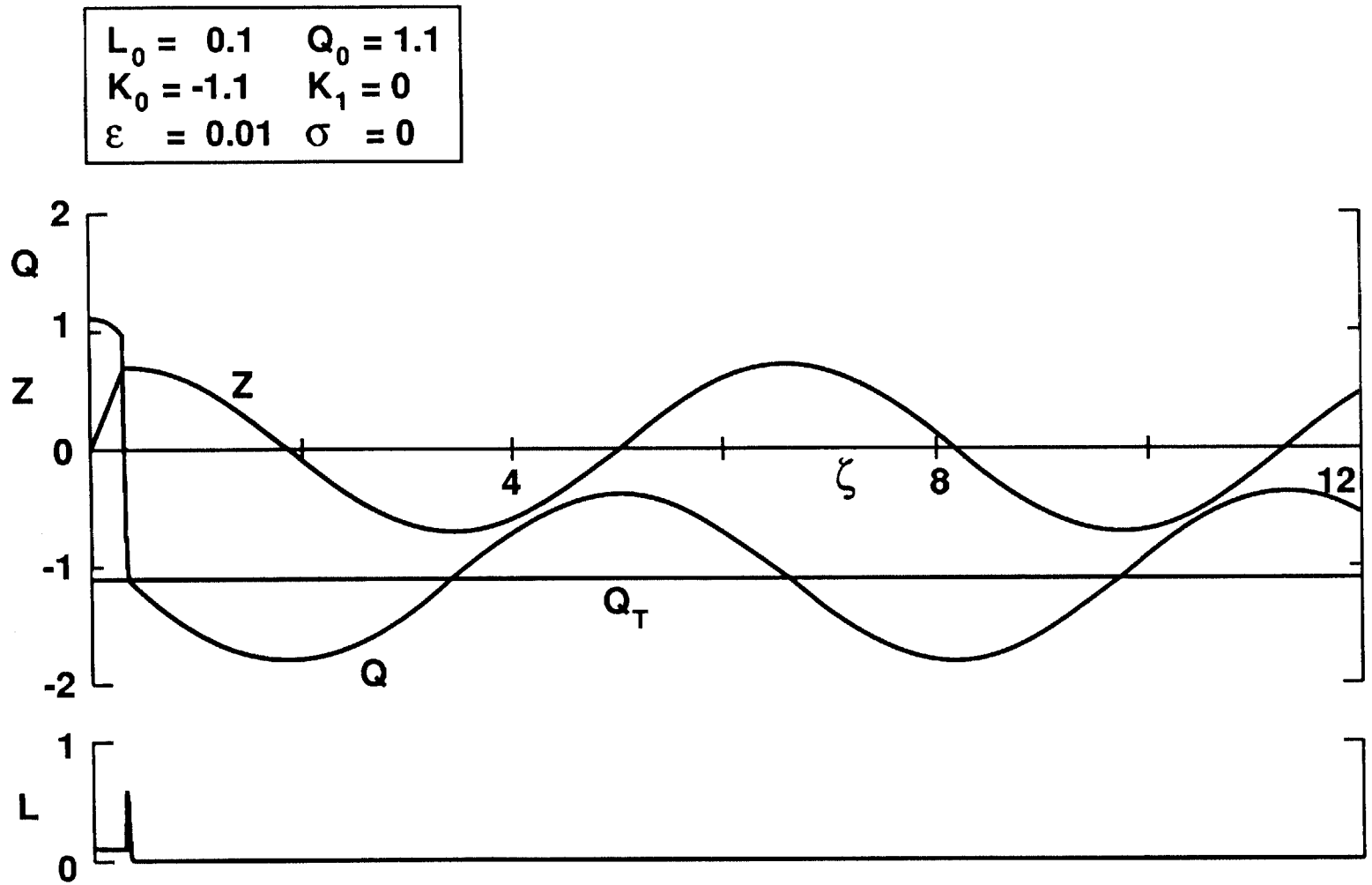

Figure 4.6 Solution when throttle abruptly closed.

Fig. 4.6 ART

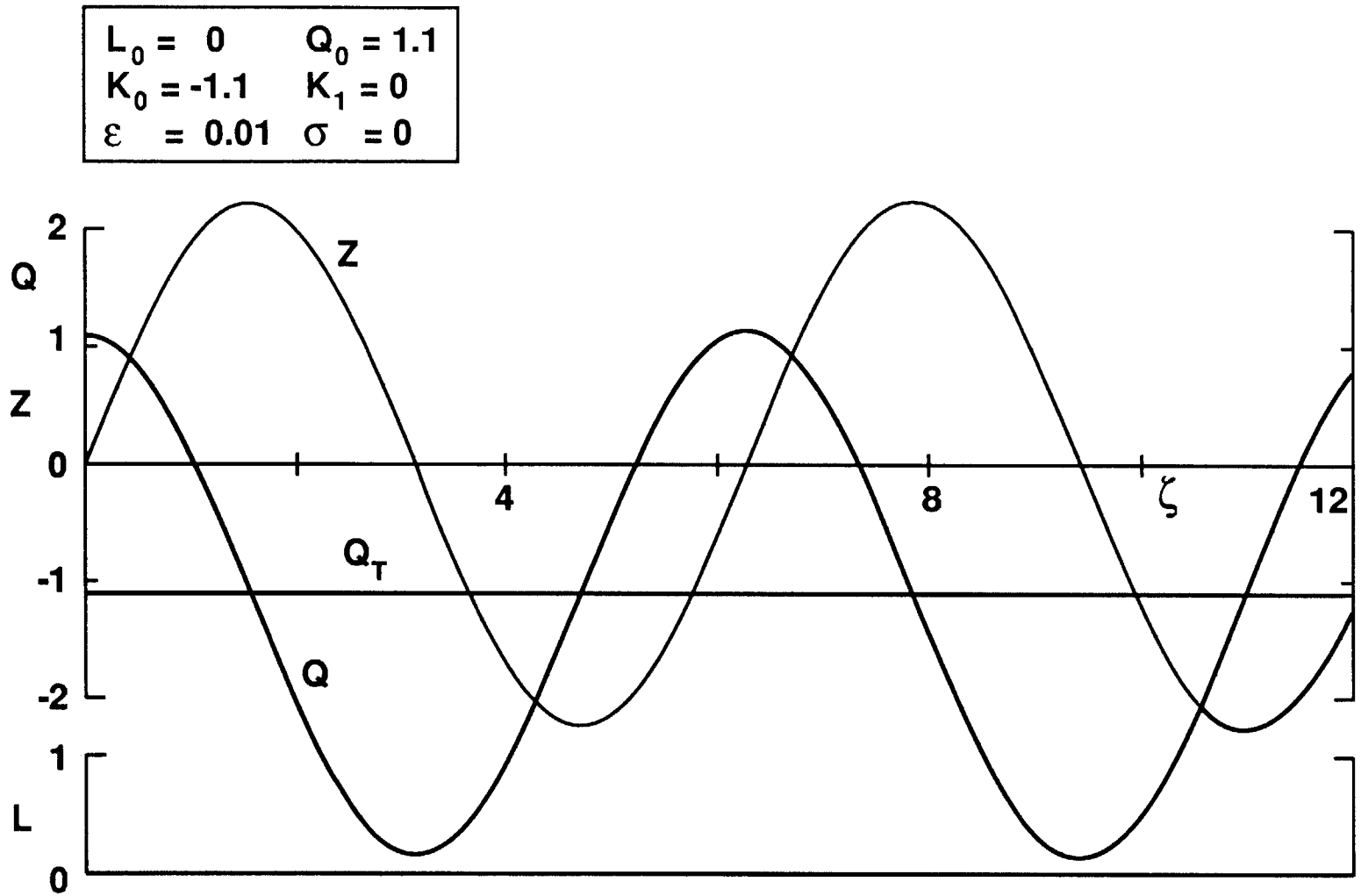

Figure 4.7 Same as previous Figure, except that resonance suppressed by holding L = 0.

Fig. 4.7 ART

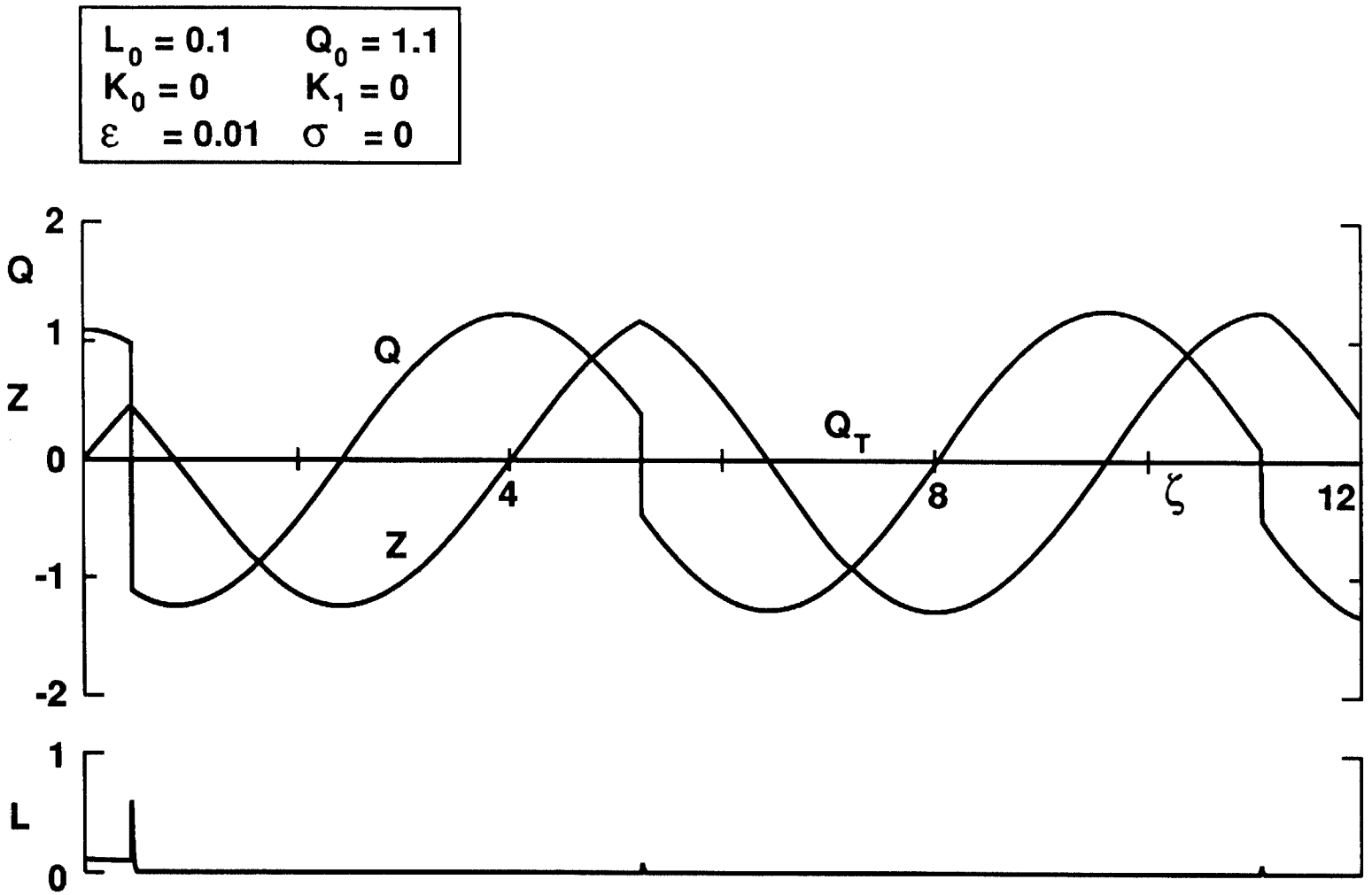

Figure 4.8 Solution for abrupt throttle closure, but only to Q = 0.

Fig. 4.8 ART

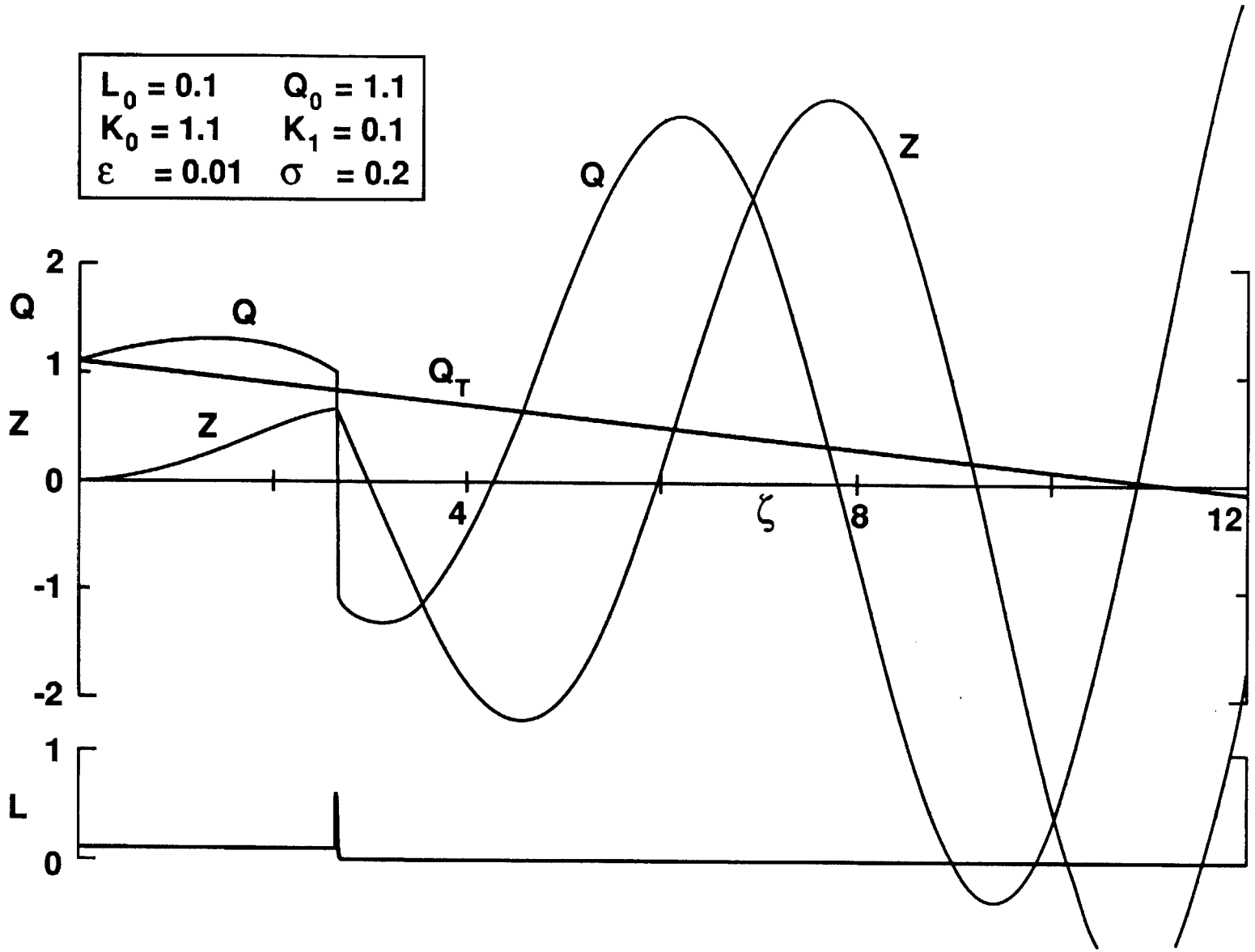

Figure 4.9 Effect of a positive (unstable) slope of the characteristic when the throttle is gradually closed.

Fig. 4.9 ART

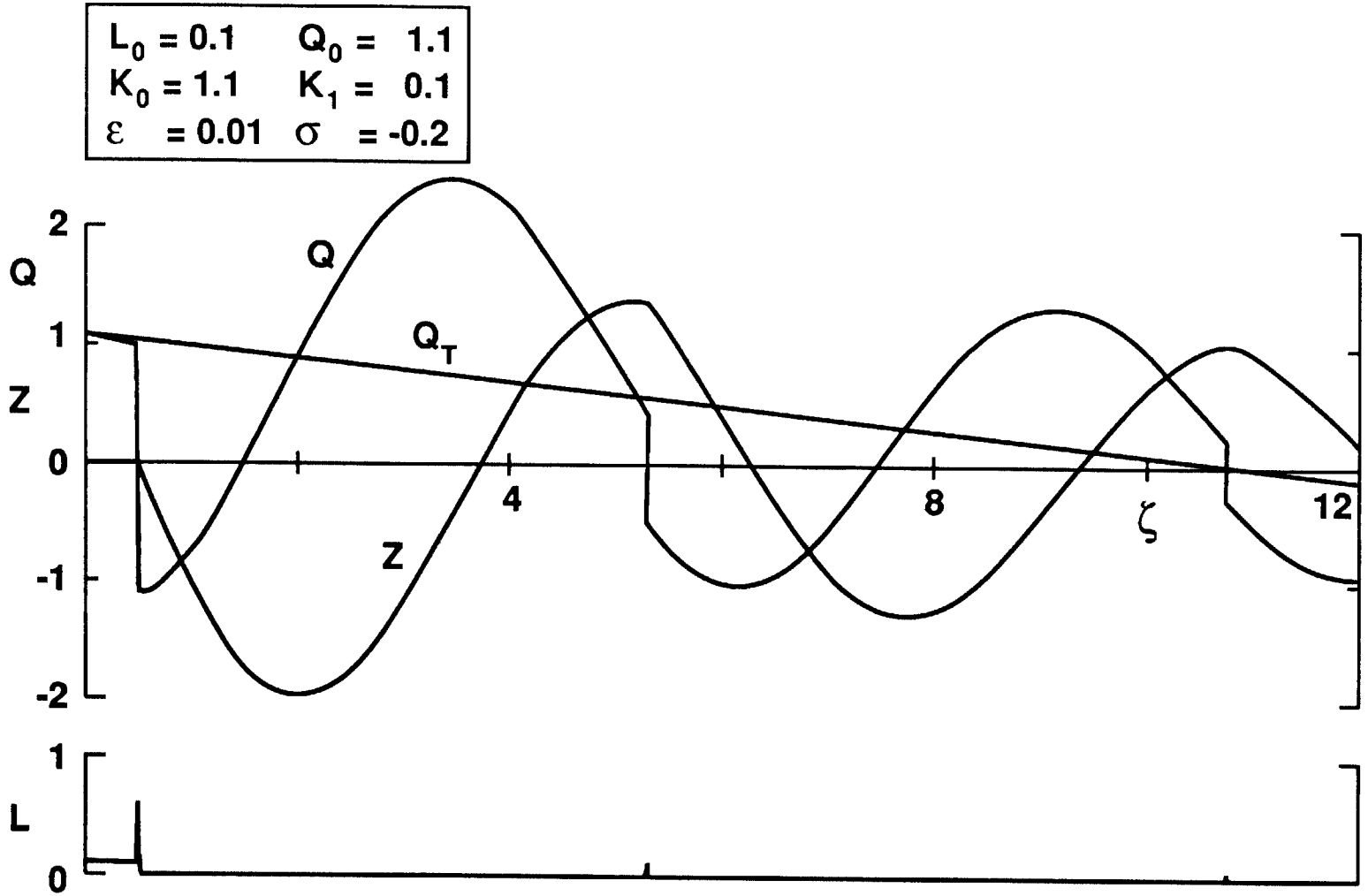

Figure 4.10 Same as previous Figure, except that characteristic slope is negative (stable).

Fig. 4.10 ART

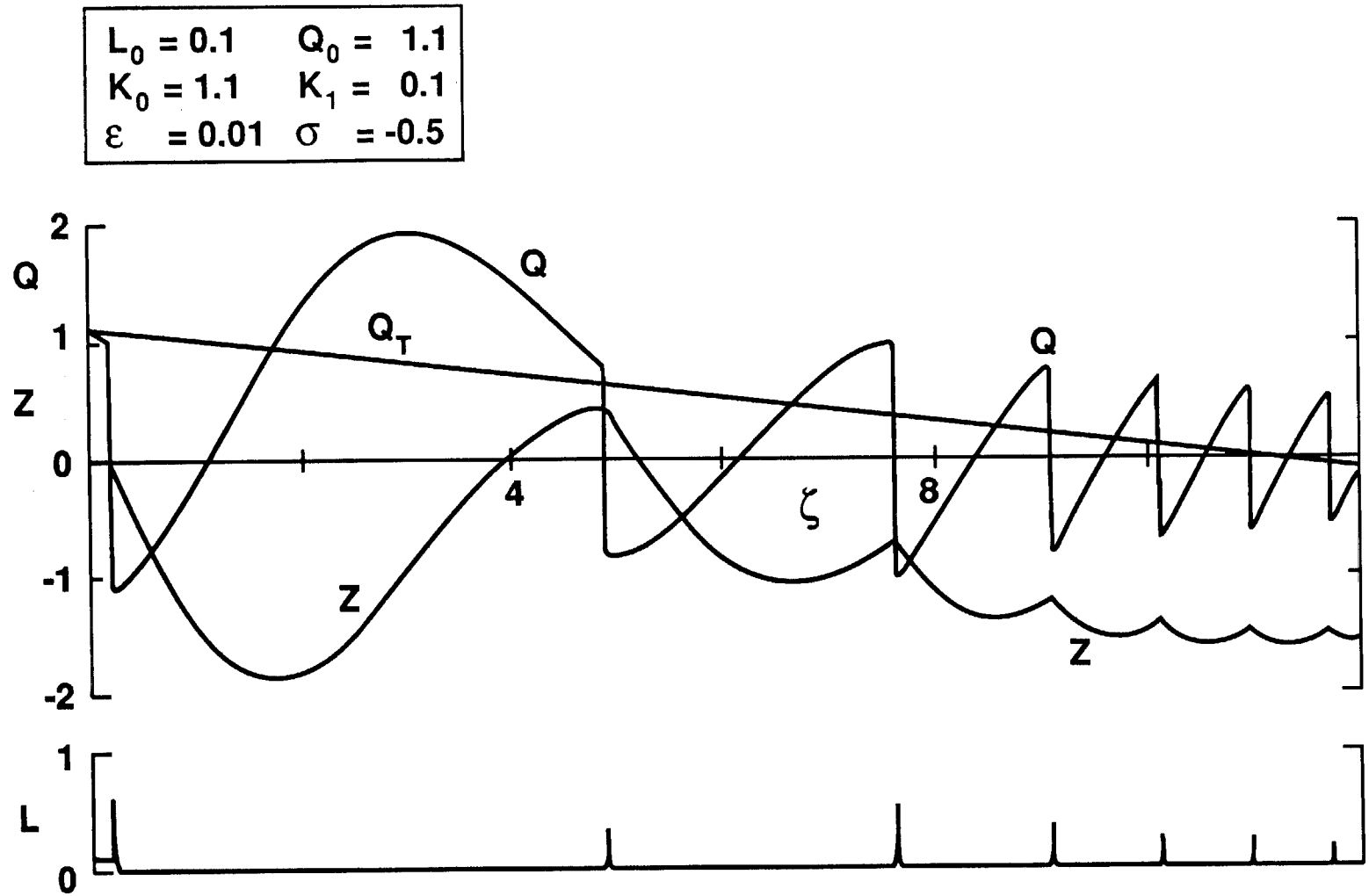

Figure 4.11 Conditions as in previous Figure, except that characteristic slope is more negative (more stable).

Fig. 4.11 ART

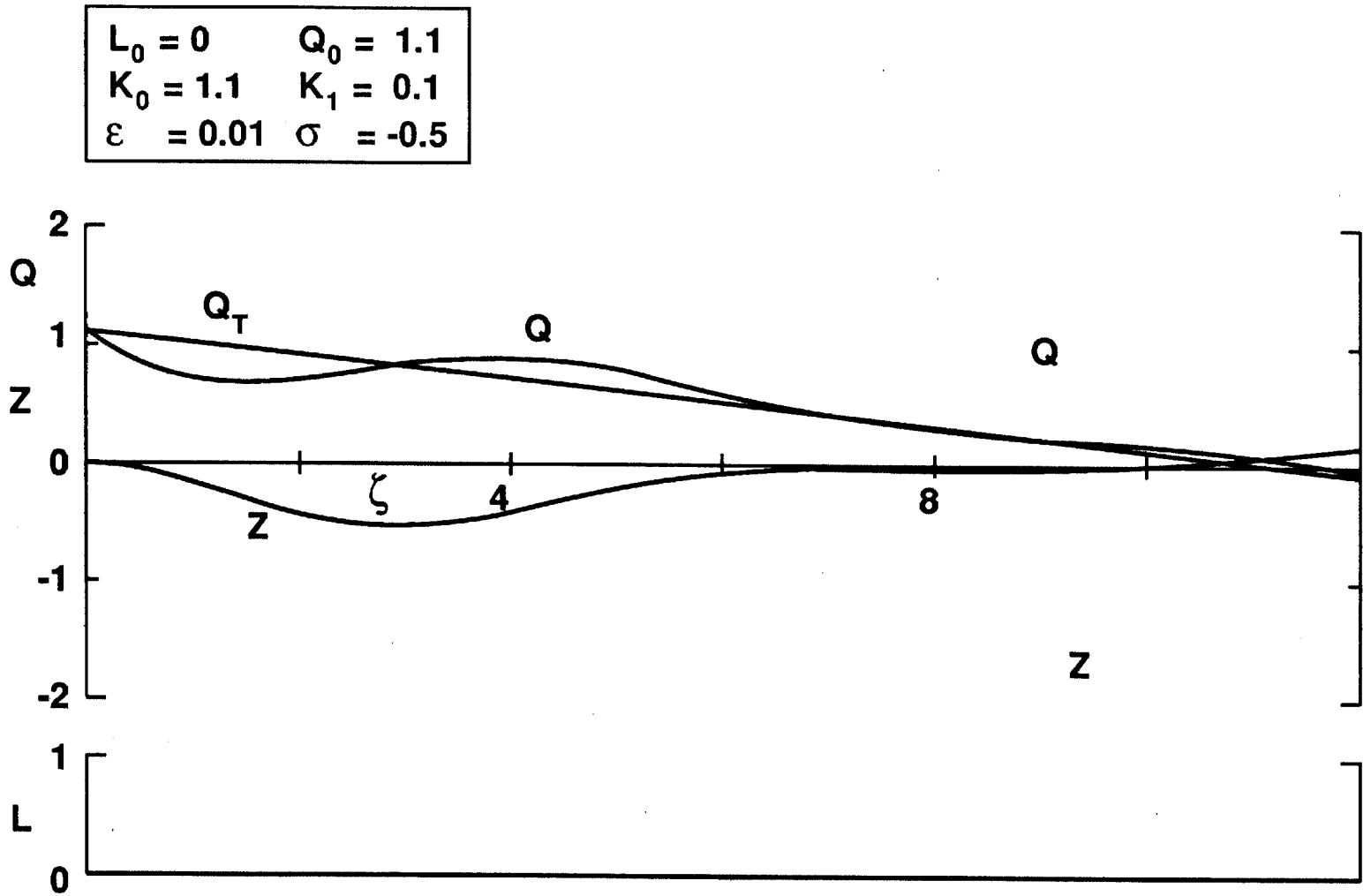

Figure 4.12 Conditions as in previous Figure, except that resonance is prevented by holding L = 0.

Fig. 4.12 ART

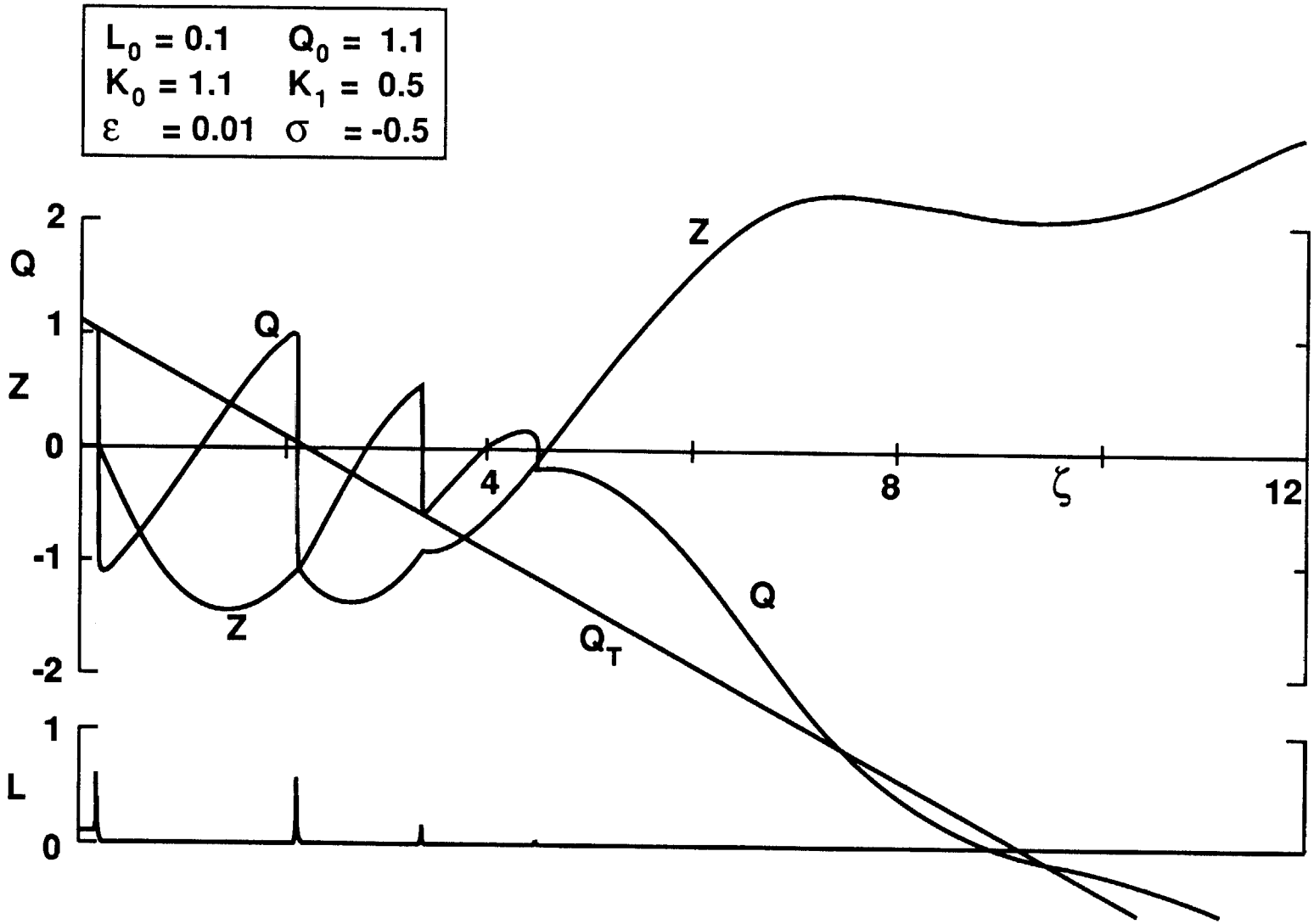

Figure 4.13 Same as Figure 4.11 except that throttle is closed more rapidly.

Fig. 4.13 ART

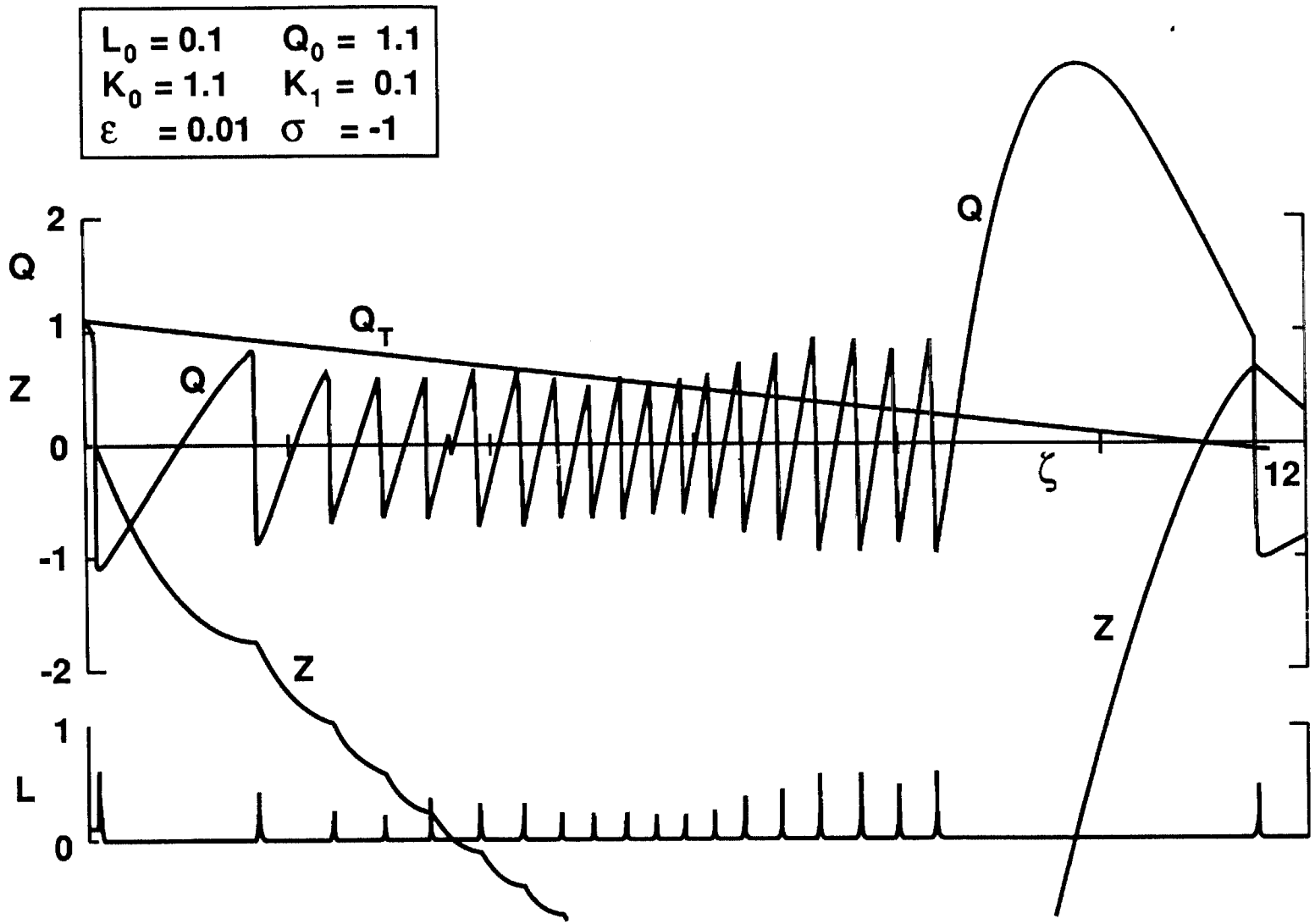

Figure 4.14 Same conditions as Figure 4.11, except that the characteristic slope is still more negative.

Fig. 4.14 ART

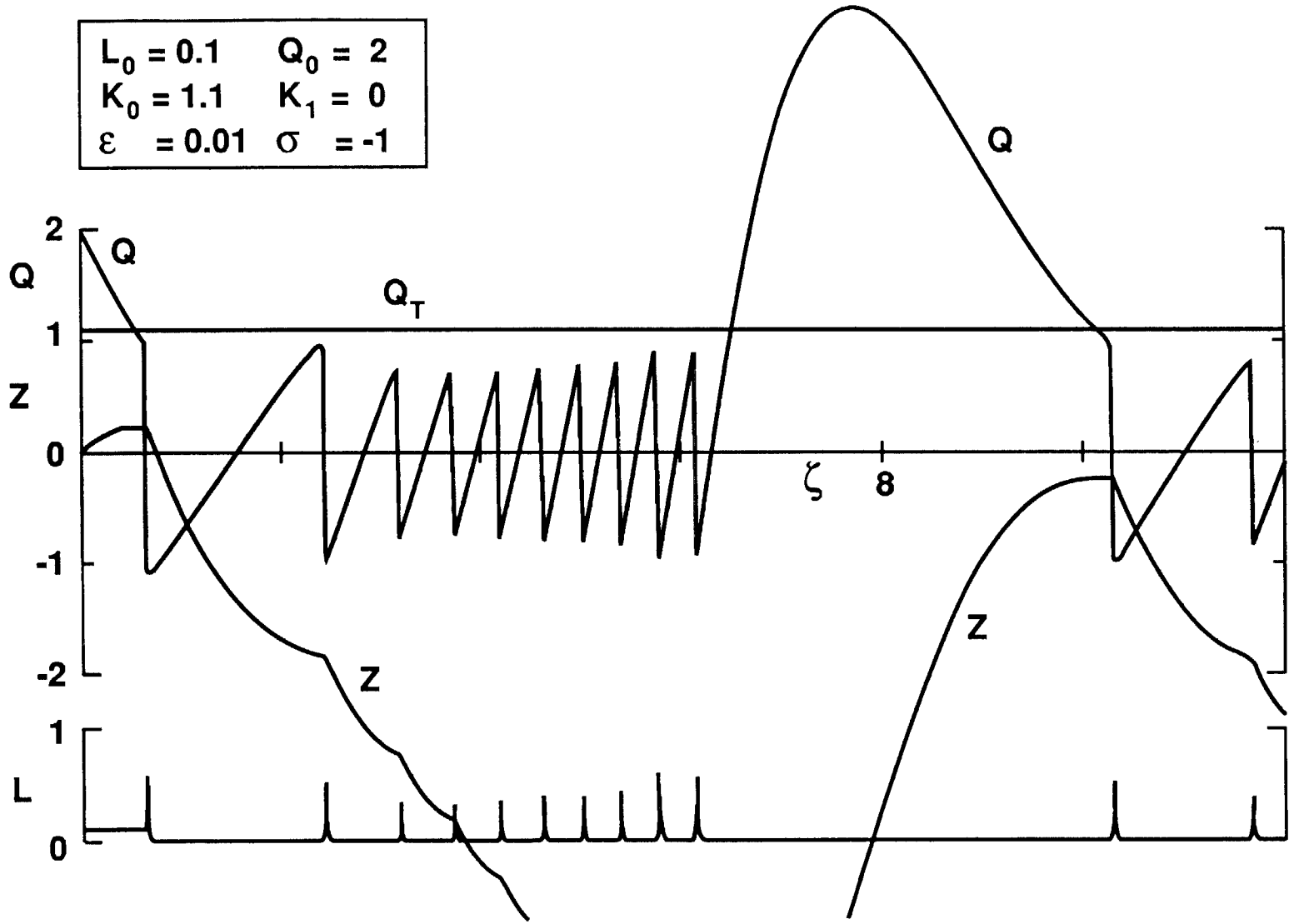

Figure 4.15 Resonant capture; throttle above amplification level and characteristic slope highly negative (stable)

Fig. 4 15 ART

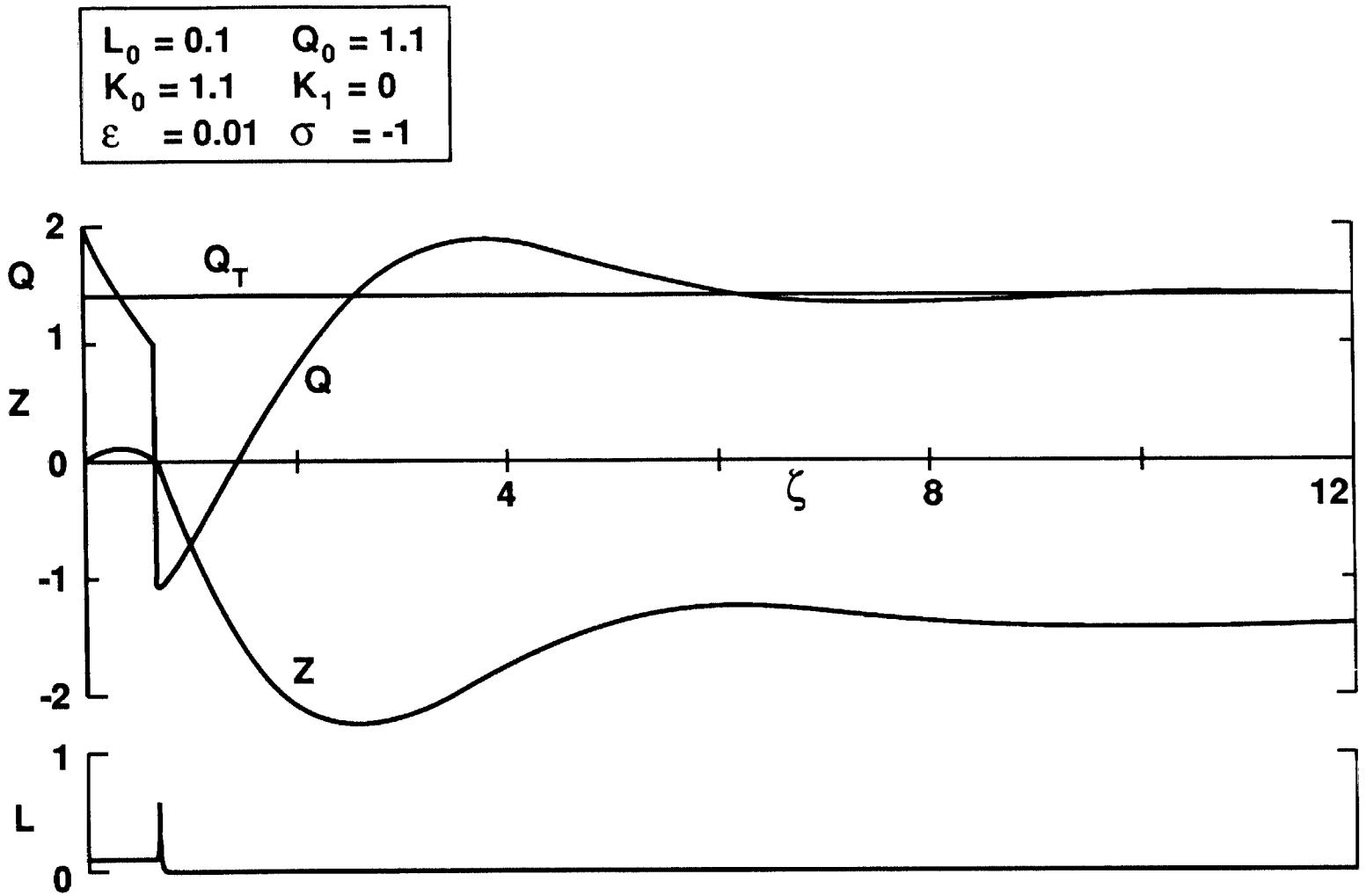

Figure 4.16 Resonant capture; same as previous Figure except that throttle is set higher above amplification level.

Fig 4.16 ART

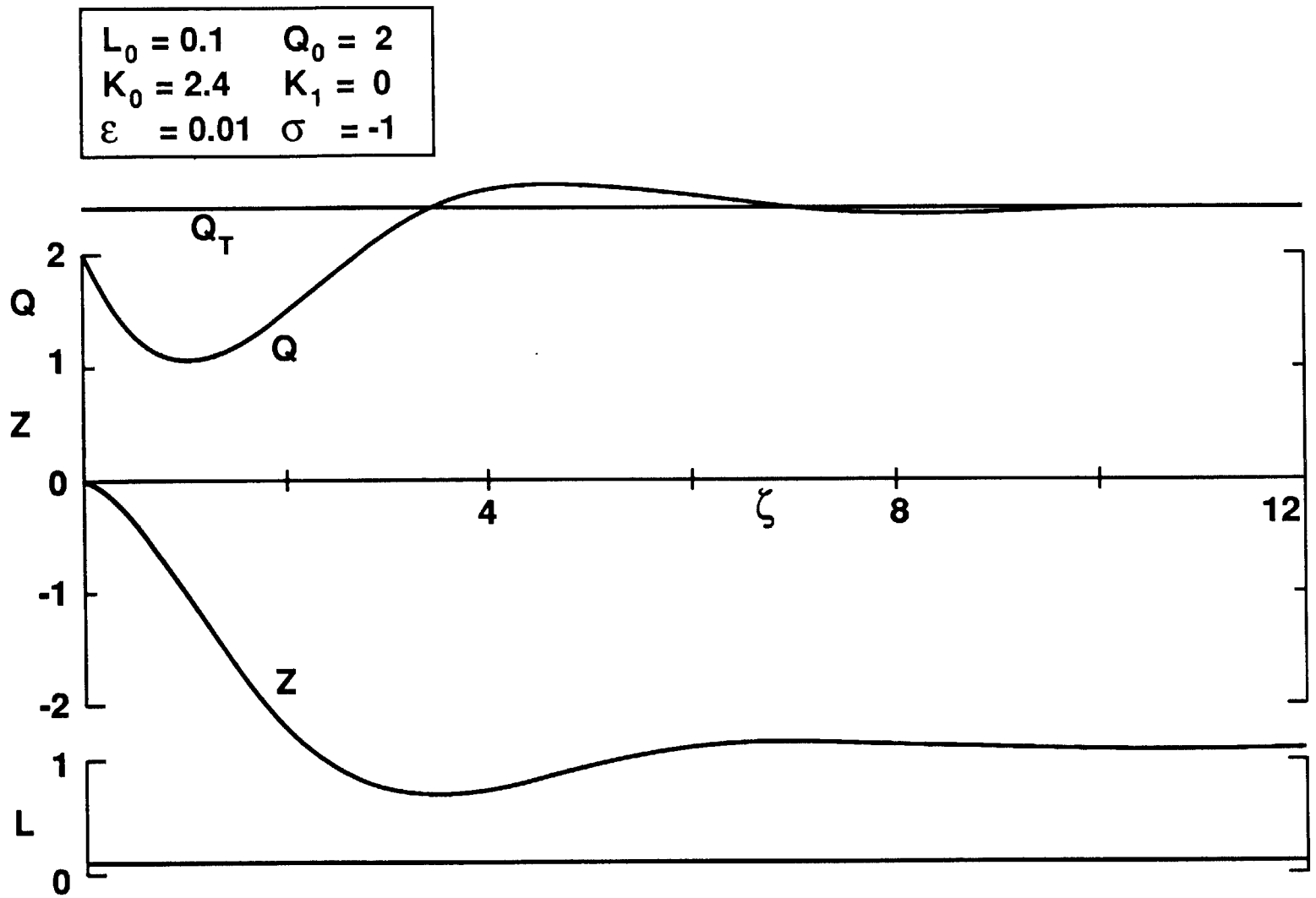

Figure 4.17 Resonant capture; same as previous Figure except that throttle is set higher above amplification level.

Fig. 4.17 ART

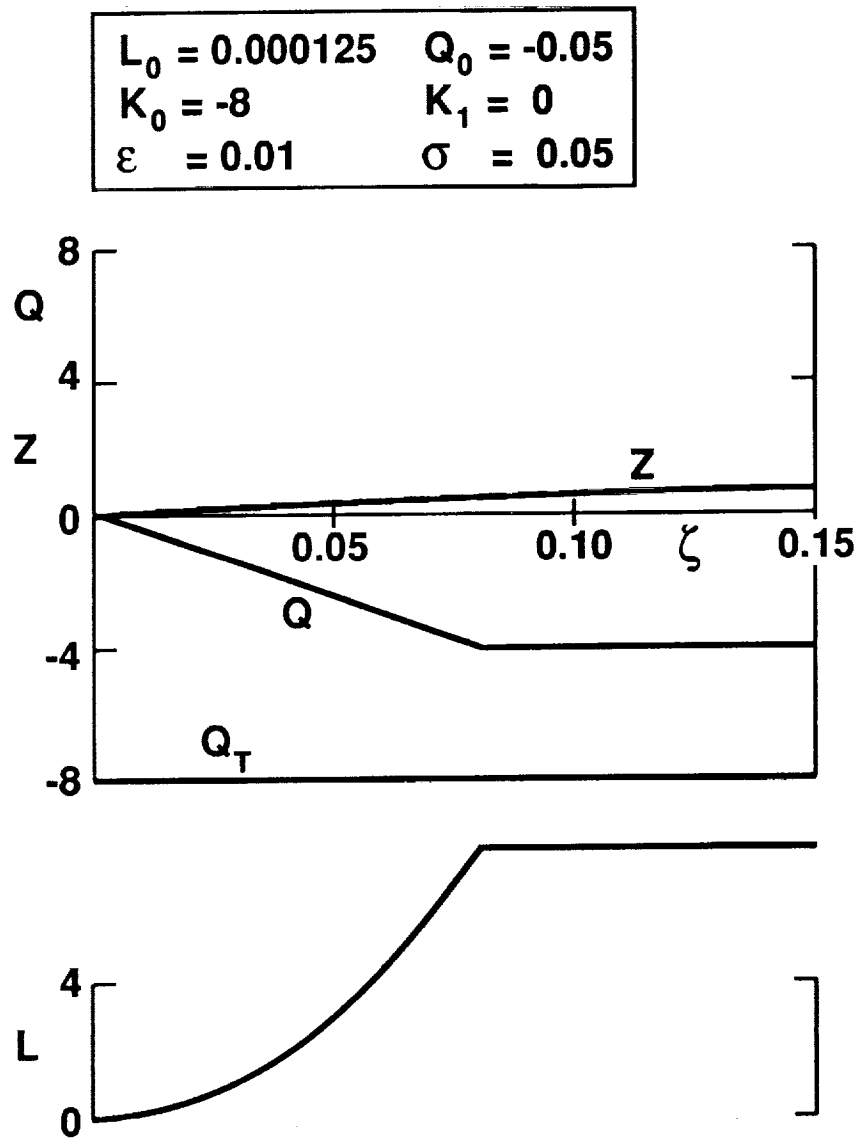

Figure 4.18 Inner solution appropriate for higher circumferential modes such as 3rd or 4th.

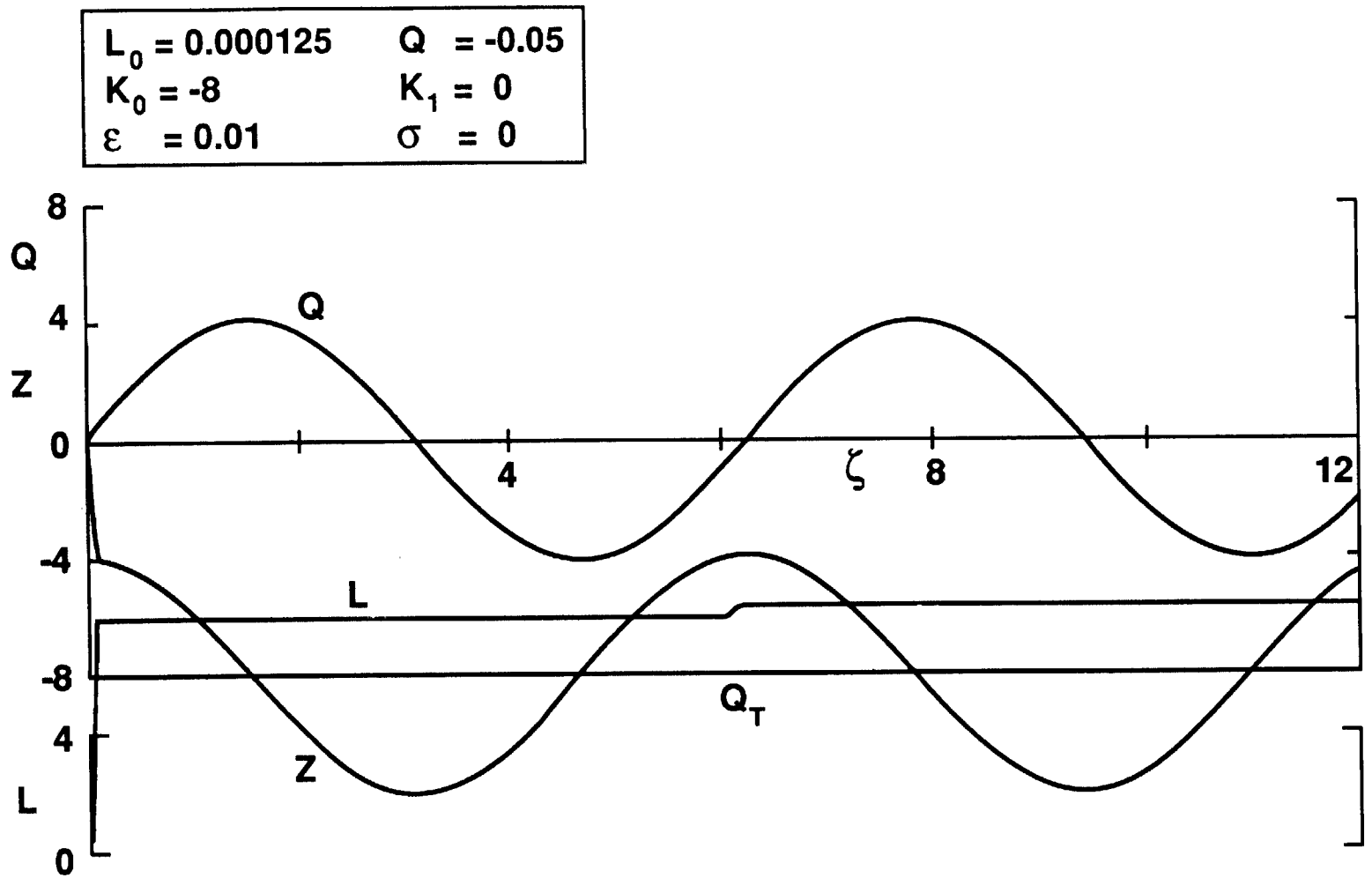

Figure 4.19 Development of surge for amplification typical of higher harmonics, with zero (neutral) characteristic slope.

Fig 4.19 ART

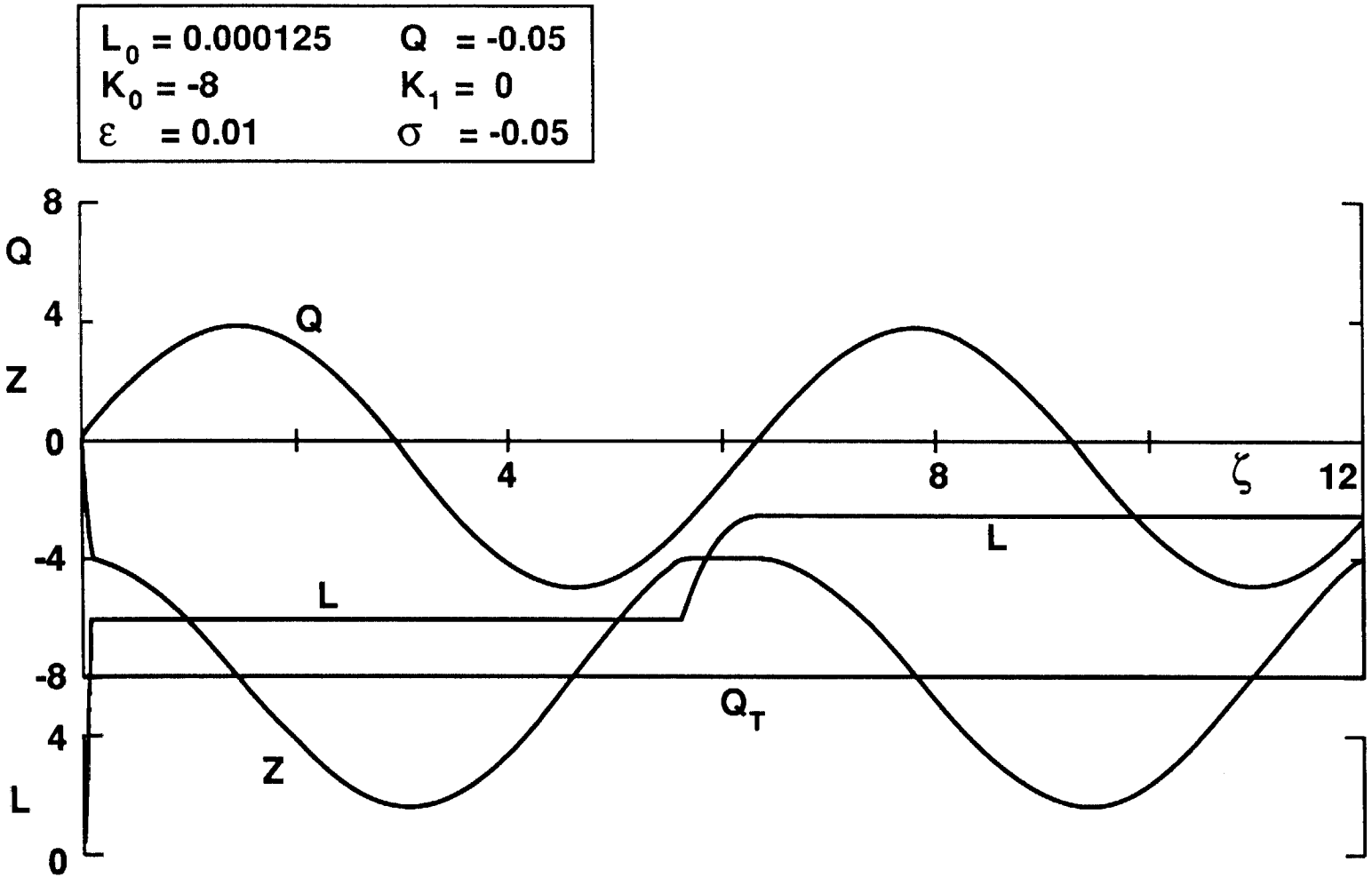

Figure 4.20 Development of surge disturbance for amplification typical of higher harmonics, for a slightly negative (stable) characteristic slope.

Fig. 4.20 ART

APPENDIX A

In [1], owing to length limitations, the solution of the small-perturbation equations was presented only for parallel diffuser walls (n = 0) and the first circumferential mode (b = 1). For the record, the general solution for any n and any b is described in this Appendix. The correspondence with equations in [1] will be noted, and, where possible, the same notation will be used, with the caret (^) applied to specify quantities arising in that linear analysis. However, in this report, Φ rather than V is used to denote mean flow coefficient. Certain new quantities j, x, y, μ, and ν appear only in this Appendix; they are defined in the text below.

The applicable inviscid equations for flow in the diffuser are recorded in Eqs. (3.17)-(3.19). Small perturbations are assumed, in terms consistent with Eqs. (3.20) and (3.21), and with Eqs. (6)-(8) of [1]:

$$\frac{v}{U} = \frac{\Phi}{r} + \hat{A}\, e^{ib\tilde{\theta}} \; ; \quad \frac{w}{U} = \hat{W}\, e^{ib\tilde{\theta}} \; ; \quad {}_dP = \hat{P}\, e^{ib\tilde{\theta}} \tag{A.1}$$

The three Euler equations for small disturbances then become, instead of Eqs. (9)-(11) of [1],

$$Vr^n \left[r\hat{A}_r - (1 - n)\,\hat{A}\right] + ib\,(1 - fr^2)\hat{A} - 2\hat{W} + r^2\hat{P}_r = 0 \tag{A.2}$$

$$Vr^n(r\hat{W}_r + \hat{W}) + ib\,(1 - fr^2)\,\hat{W} + ir\,\hat{P} = 0 \tag{A.3}$$

$$r\,\hat{A}_r + (1 - n)\,\hat{A} + i\,b\,\hat{W} = 0 \tag{A.4}$$

The boundary conditions corresponding to Eq. (12)-(14) of [1] are now, at the diffuser entrance (r = 1),

$$\hat{A}(1) = 1 \quad ; \hat{W}\,(1) = 0 \tag{A.5}$$

and at the diffuser exit ($r = r_F$),

$$\hat{P}\,(r_F) = 0 \tag{A.6}$$

The foregoing equations reduce to those in [1] if n and b are set equal to 0 and 1, respectively.

The solution of this system of equations for P, A, and W has the following form (only P was given in Eq. (15) of [1]):

$$b\hat{P} = [\hat{K}_1 \hat{P}_1 - \hat{K}_2 \hat{P}_2 - \hat{PP}_1] + i\ [\hat{K}_2 \hat{P}_1 + \hat{K}_1 \hat{P}_2 - \hat{PP}_2] \tag{A.7}$$

$$\hat{A} = r\,[\hat{K}_1 (y_1 j_3 - y_2 j_1) - \hat{K}_2 (y_1 j_4 - y_2 j_2)] + (\mu + 1 - n)\, r\, y_1 + (\mu + 1)\, r\, j_2 + ir\,[\hat{K}_2 (y_1 j_3 - y_2 j_1) + \hat{K}_1 (y_1 j_4 - y_2 j_2)] \tag{A.8}$$

$$b\hat{W} = \hat{K}_1\,[(\mu + 1)\, y_1 j_4 + (\mu + 1 - n)\, y_2 j_2] + \hat{K}_2\,[(\mu + 1)\, y_1 j_3 + (\mu + 1 - n)\, y_2 j_1] + i\,\{ -\hat{K}_1\,[(\mu + 1)\, y_1 j_3 + (\mu + 1 - n)\, y_2 j_1] + \hat{K}_2\,[(\mu + 1)\, y_1 j_4 + (\mu + 1 - n)\, y_2 j_2] + r\,(y_2 - y_1)\} \tag{A.9}$$

where, corresponding to Eqs.(16)-(18) of [1], the following definitions apply:

$$\hat{P}_1 = \frac{\Phi}{b}\,[\cos \hat{z} - b^2\, r^n\, (y_1 j_3 - y_2 j_1)] - (1 - fr^2)\,[(\mu + 1)\, y_1 j_4 + (\mu + 1 - n)\, y_2 j_2] \tag{A.10}$$

$$\hat{P}_2 = \frac{\Phi}{b}\,[\sin \hat{z} - b^2 r^n\, (y_1 j_4 - y_2 j_2)] + (1 - fr^2)\,[(\mu + 1)\, y_1 j_3 + (\mu + 1 - n)\, y_2 j_1] \tag{A.11}$$

$$\hat{PP}_1 = \frac{\Phi}{b}\, r^n\, b^2\,[(\mu + 1)\, y_2 + (\mu + 1 - n)\, y_1] \tag{A.12}$$

$$\hat{PP}_2 = b^2 (1 - fr^2)\, (y_2 - y_1) \tag{A.13}$$

Two parameters involve n and b:

$$\mu = -1 + \frac{n}{2} + \sqrt{b^2 + \frac{n^2}{4}} \tag{A.14}$$

$$\nu = n - 3 - 2\mu \tag{A.15}$$

and certain functions have the definitions which follow.

$$\hat{z} = \left(\frac{r^{-n}}{n} + f\frac{r^{2-n}}{2-n}\right)\frac{b}{\Phi} \quad \text{if } n \neq 0 \tag{A.16}$$

$$\hat{z} = \left(\ln r + \frac{1}{2}fr^2\right)\frac{b}{\Phi} \quad \text{if } n = 0 \tag{A.17}$$

$$y_1 = -\frac{r^{\nu+\mu}}{\nu+1} \tag{A.18}$$

$$y_2 = -\frac{r^{\mu-1}}{\nu+1} \tag{A.19}$$

It may be noted that $\hat{z}$ is the same as ϑ defined in Eq. (4.8) when f = 0.

The following integrals require numerical evaluation, in which x denotes the variable of integration from 1 to r:

$$j_1 = \int_1^r x^{-(\mu+n)} \cos \hat{z}(x)\, dx \tag{A.20}$$

$$j_2 = \int_1^r x^{-(\mu+n)} \sin \hat{z}(x)\, dx \tag{A.21}$$

$$j_3 = \int_1^r x^{-(3n - 1 + \nu)/2} \cos \hat{z}(x)\, dx \tag{A.22}$$

$$j_4 = \int_1^r x^{-(3n - 1 + \nu)/2} \sin \hat{z}(x)\, dx \tag{A.23}$$

Inspection shows that the solution just described automatically satisfies the boundary conditions (Eq. (A.5) at the diffuser entrance. Those conditions require modification [1] if the rotor blades are not radial at the rotor exit, of course. The constants $\hat{K}_1$ and $\hat{K}_2$ may be chosen to satisfy the boundary condition at the diffuser exit, Eq. (A.6), with these results:

$$\hat{K}_1 = \left[(\hat{P}_1 \hat{PP}_1 + \hat{P}_2 \hat{PP}_2)/(\hat{P}_1^2 + \hat{P}_2^2)\right]_{r = r_F} \quad \text{(A.24)}$$

$$\hat{K}_1 = \left[(\hat{P}_1 \hat{PP}_2 - \hat{P}_2 \hat{PP}_1)/(\hat{P}_1^2 + \hat{P}_2^2)\right]_{r = r_F} \quad \text{(A.25)}$$

The latter boundary condition is changed if there is any recovery of dynamic head at the diffuser exit, as explained in [1].

NOTATION

The notation in this Report is consistent with that in [1] and [4], because the analysis is, in effect, an amalgamation of those previous two papers. All lengths are in ratio to the radius of the diffuser inlet (rotor discharge).

A amplitude of cosine part of circumferential wave of radial velocity disturbance, Eqs. (3.10), (3.20)

A_f effective flow area

AM imaginary part of disturbance A in [1], Eq. (3.35)

AR real part of disturbance A in [1], Eq. (3.35)

a reciprocal time-lag parameter of blade passage, Eq. (3.4)

B amplitude of sine part of velocity disturbance, Eq. (3.20)

B_g inertia parameter for surge ("Greitzer's B")

b mode number for circumferentially-traveling wave

b* pole strength for pressure disturbance, Eq. (4.20)

c* pole strength for integral, Eq. (4.20)

F_T throttle characteristic function, Eq. (3.8)

f coefficient of propagation speed of circumferential disturbance, in laboratory frame, Eq. (3.12)

G function of exit radius and flow coefficient defined in Eq. (4.9)

g disturbance of axial flow coefficient, Eq. (3.5)

H height parameter of cubic axisymmetric characteristic, Fig. 3.1

I integral expression defined in Eq. (4.17)

J square of disturbance wave amplitude at diffuser entrance, Eq. (3.39)

K_0 ititial throttle setting, Eq. (4.46)

K_1 rate of throttle closure, Eq. (4.46)

k constant in "inner" solution, Eq. (4.41)

L amplitude of circumferential disturbance of radial velocity, Eq. (4.32)

L_0 initial value of L

l diffuser width, Eq. (2.1) and Fig. 2.1; generally a function of radius

l_I length of inlet section before rotor, Fig. 1 of [4]

l_c effective flow length of system up to rotor exit, Eq. (3.4)

M function of exit radius and flow coefficient defined in Eq. (4.10)

m duct-flow parameter of rotor entrance, Eq. (3.6)

n exponent describing diffuser convergence, Eq. (2.1)

p static pressure in diffuser

p_F plenum pressure to which diffuser discharges

p_T upstream total pressure

P pressure coefficient, Eq. (3.7)

$\bar{P}$ angle-averaged pressure coefficient, Eq. (3.7)

$\bar{P}_{qs}$ quasi-steady pressure coefficient

$_dP$ wave-like part of pressure coefficient, Eq. (3.7)

$_1P$ amplitude of cosine part of pressure wave, Eq. (3.11)

$_2P$ amplitude of sine part of pressure wave, Eq. (3.11)

PM imaginary part of pressure-wave amplitude from [1]

PR real part of pressure-wave amplitude from [1]

Q nonlinear disturbance of flow coefficient, Eq. (4.32)

q nonlinear disturbance of flow coefficient, Eq. (4.24)

r radial coordinate (relative to radius of diffuser inlet)

r_F radius at diffuser exit; radius ratio of diffuser, Fig. 1.1

S shut-off parameter of cubic axisymmetric characteristic, Fig. 3.1

SL local slope of compressor characteristic, (Eq. (4.21)

t time

U wheel speed at rotor exit (diffuser inlet)

v radial velocity in diffuser

W width parameter of cubic axisymmetric characteristic, Fig. 3.1

w circumferential velocity in diffuser

X second-order swirl, Eq. (3.21)

Y potential for wave-like velocity disturbance, Eq. (3.5)

Z nonlinear disturbance of pressure-rise coefficient, Eq. (4.32)

z nonlinear disturbance of pressure-rise coefficient, Eq. (4.25)

α coefficient in analysis for f = 0, Eqs. (4.2)-(4.4)

β coefficient in analysis for f = 0, Eqs. (4.2)-(4.4)

γ coefficient in analysis for f = 0, Eqs. (4.2)-(4.4)

ε initial small disturbance of flow coefficient, Eq. (4.32)

λ strength of wave disturbance, (Eq. (4.26)

Φ flow coefficient based on velocity at rotor exit and wheel speed there

Ψ actual pressure-rise coefficient, Eq. (3.3)

ψ_c axisymmetric characteristic function, Eq. (3.13)

ψ_{c0} height parameter of axisymmetric characteristic function, Eq. (3.13)

θ circumferential angle coordinate, laboratory frame

$\tilde{\theta}$ angle coordinate in frame of traveling wave, Eq. (3.12)

ϑ function of exit radius and flow coefficient, Eq. (4.8)

ρ density

σ redefined slope of characteristic, Eq. (4.28)

τ blade-passage lag coefficient

ξ time coordinate; rotor travels one radian in unit time

ζ redefined time coordinate, Eq. (4.27)

ζ' "inner" time variable, ζ/ε

Superscripts

* at resonance

^ obtained from the linear analysis of [1]

(1) identifies traveling mode in Eqs. (5.1), (5.2)

(2) identifies traveling mode in Eqs. (5.1), (5.2)

primes denote differentiation in Eqs. (4.14) and (4.15)

Subscripts

$_0$ at rotor entrance

$_1$ at diffuser entrance

$_F$ at diffuser exit

$_T$ pertaining to throttle (except p_T, which means ambient toal pressure)

partial differentiation denoted by subscripts

REFERENCES

1. Moore, F.K. "Weak Rotating Flow Disturbances, in a Centrifugal Compressor With a Vaneless Diffuser," ASME J. Turbomachinery, **111**, October1989, pp. 442-449.

2. Moore, F.K. "A Theory of Rotating Stall of Multistage Compressors: Part I--Small Disturbances," ASME J. Eng. for Power, **106**, April 1984, pp. 313-321.

3. van den Braembussche, R., "Rotating Stall in Vaneless Diffusers of Centrifugal Compressors," Tech. Note 145, von Karman Institute for Fluid Dynamics, Rhode Ste Genese, Belgium, June 1982.

4. Moore, F.K., and Greitzer, E.M., "A theory of Post-Stall Transients on Axial Compression Systems: Part I--Development of Equations," ASME J. Eng. for Gas Turb. and Power, **108**, January1986, pp 68-76.

NASA
National Aeronautics and Space Administration

Report Documentation Page

1. Report No.	2. Government Accession No.	3. Recipient's Catalog No.
NASA CR-187049		

4. Title and Subtitle	5. Report Date
Theory of Finite Disturbances in a Centrifugal Compression System with a Vaneless Radial Diffuser	December 1990
	6. Performing Organization Code

7. Author(s)	8. Performing Organization Report No.
F.K. Moore	None
	10. Work Unit No. 535-05-10

9. Performing Organization Name and Address	11. Contract or Grant No.
Cornell University Ithaca, New York 14853	NAG3-349
	13. Type of Report and Period Covered Contractor Report Final

12. Sponsoring Agency Name and Address	14. Sponsoring Agency Code
National Aeronautics and Space Administration Lewis Research Center Cleveland, Ohio 44135-3191	

15. Supplementary Notes

Project Manager, Daniel H. Buffum, Propulsion Systems Division, NASA Lewis Research Center.

16. Abstract

A previous small-perturbation analysis of circumferential waves in circumferential compression systems, assuming inviscid flow, is shown to be consistent with observations that narrow diffusers are more stable than wide ones, when boundary-layer displacement effect is included. The Moore-Greitzer analysis for finite-strength transients containing both surge and rotating stall in axial machines is adapted for a centrifugal compression system. Under certain assumptions, and except for a new, second-order swirl, the diffuser velocity field, including resonant singularities, can be carried over from the previous inviscid, linear analysis. Nonlinear transient equations are derived and applied in a simple example to show that throttling through a resonant value of flow coefficient must occur in a sudden surge-like drop, accompanied by a transient rotating wave. This "inner" solution is superseded by an "outer" surge response on a longer time scale. Surge may occur purely as result of circumferential-wave resonance. Numerical results are shown for various parametric choices relating to throttle schedule and the characteristic slope. For higher circumferential modes, a somewhat different picture of the amplification process seems appropriate, and suggestions are made about the effects of resonance in such cases. The problem of considering a number of circumferential modes simultaneously is briefly discussed.

17. Key Words (Suggested by Author(s))	18. Distribution Statement
Compressor; Stability; Centrifugal; Stall; Surge; Resonance; Diffuser	Unclassified – Unlimited Subject Category 07

19. Security Classif. (of this report)	20. Security Classif. (of this page)	21. No. of pages	22. Price*
Unclassified	Unclassified	66	A04

NASA FORM 1626 OCT 86

*For sale by the National Technical Information Service, Springfield, Virginia 22161